THE UNIVERSITY OF CHICAGO

HIPPOCAMPAL COGNITIVE MAP DYNAMICS: INVESTIGATING THE FATE AND REPLAY OF PLACE CELLS

A DISSERTATION SUBMITTED TO
THE FACULTY OF THE DIVISION OF THE PHYSICAL SCIENCES
IN CANDIDACY FOR THE DEGREE OF
DOCTOR OF PHILOSOPHY

DEPARTMENT OF PHYSICS

BY
YU HUNG CHIU

CHICAGO, ILLINOIS
DECEMBER 2023

This thesis is dedicated to my parents KinMan Chiu and IokTin Leung

TABLE OF CONTENTS

LIST OF FIGURES

LIST OF TABLES

ACKNOWLEDGMENTS

First and foremost, I would like to express my utmost gratitude to my advisor Dr. Mark Sheffield for giving me the opportunity, guidance and support. As a physics graduate with no background in neuroscience, Mark was so kind to accept me as a member of the lab. He shared his understanding in the field and guided me through literature when things are completely new to me. I learned a lot from him. Mark has been giving me incredible support, patience and tolerance throughout the whole project. The manuscript won't be possible without his support. I can't be more lucky to have Mark as my advisor.

I also want to thank every member of the Sheffield lab. The atmosphere is so welcoming and positive. I would like to particularly thank Can, Seetha and Heather, for sharing their data with me, letting me analyze them, and answering all my annoying petty questions. I also want to thank Antoine and Doug, for providing lots of insightful comments on the project and the manuscript.

I am grateful to my thesis committee member: Dr. Jason MacLean, Dr. Staphanie Palmer, and Dr. Heinrich Jaeger, for agreeing to be on the committee even though they are very busy, and very importantly their inputs and insights.

My gratitude also goes to my previous advisor, Dr Paul Wiegmann, for taking me as a student and guiding me through the field of condensed matter physics. Though I no longer work in the field, his word of wisdom has helped me a lot in my life.

I want to thank the Department of Physics for the support they gave me. I want to thank Dr. David Reid and Dr. Zosia Krusberg for all the discussions and support. I can't be more grateful to Putri Kusumo for all the coordination. Dr. Stuart Gazes has been very supportive in coordinating TA position for me. And it is always a pleasure to work with the Physics teaching lab staff Dr. Mark Chantell, Dr. David McCowan and Dr. Kevin Van de

Bogert. Their enthusiasm in teaching and the small talks in the teaching labs influences me a lot.

And I want to thank my friends and family, for all the supporting words. I won't be able to make it through without them.

ABSTRACT

The hippocampus is known to play a role in encoding, consolidating, updating and retrieving episodic memories. But the mechanism underlying these processes remains unclear. My work focuses on investigating hippocampal network and cellular dynamics in subregion CA1 during and across episodes of experience, giving insight on how memories are updated and retrieved.

We first investigated the association between the spatial preciseness of place fields (PFs) and the representational drift across sessions in the same environment. We reanalyzed data from experiments in which male mice navigated familiar and novel environments for blocks of trials across days (distinct temporal episodes), and experiments in which mice changed their reward expectation across blocks of trials (distinct internal state episodes). We found that PFs that underwent a drift across episodes showed lower spatial precision in the preceding block of trials. We suggest a conceptual model explaining the association between PF precision and drift that involves changes in CA3 input to CA1 and synaptic plasticity at CA1-CA3 synapses.

We then investigated another feature in hippocampus that is closely related to memory - place cell sequence replay. We investigated how the rate and fidelity of replay events were be modulated by reward contingencies and fear memory. We observed that replay rate dropped when reward was removed from blocks of trials and increased when reward was put back for blocks of trials. We also observed that associating an environment with an aversive shock significantly modulated the rate and fidelity of replay events.

Together these results give insight into how network and single cell dynamics within the hippocampus facilitate memory formation, consolidation and retrieval of rewarding and aversive experiences.

CHAPTER 1

INTRODUCTION

1.1 Hippocampus' role in memory

The hippocampus is known to play a role in encoding, consolidating, updating and retrieving episodic memories (Andersen et al., 2006). A famous report provided insight to the role of hippocampus in episodic memory is the case of patient H.M. (Henry Molaison). The patient underwent experimental brain surgery to relieve his epilepsy, which involved removal of hippocampus, amygdala, and surrounding structures. Unexpectedly, the patient's ability to form new episodic memories was severely impaired. His memory before the surgery, extending back into his childhood, remained intact (Scoville and Milner, 1957). This and other similar cases involving hippocampal damage had demonstrated the role of hippocampus in episodic memory.

Hippocampus also plays an important role in memory formation/consolidation/retrieval in rodents (Riedel et al., 1999; Schröder et al., 2020; Zemla and Basu, 2017). Lesions in the hippocampus impairs the rodents' ability to navigate to learned locations and their recognition of familiar environments (Morris et al., 1982; Broadbent et al., 2006). Of particular importance to this thesis, the anatomical structure of the hippocampus (Fig. 1.1) is conserved across rodents and humans. Therefore, the studies in this thesis focus on hippocampus of rodents, which can provide insights into the role of hippocampus in the human brain.

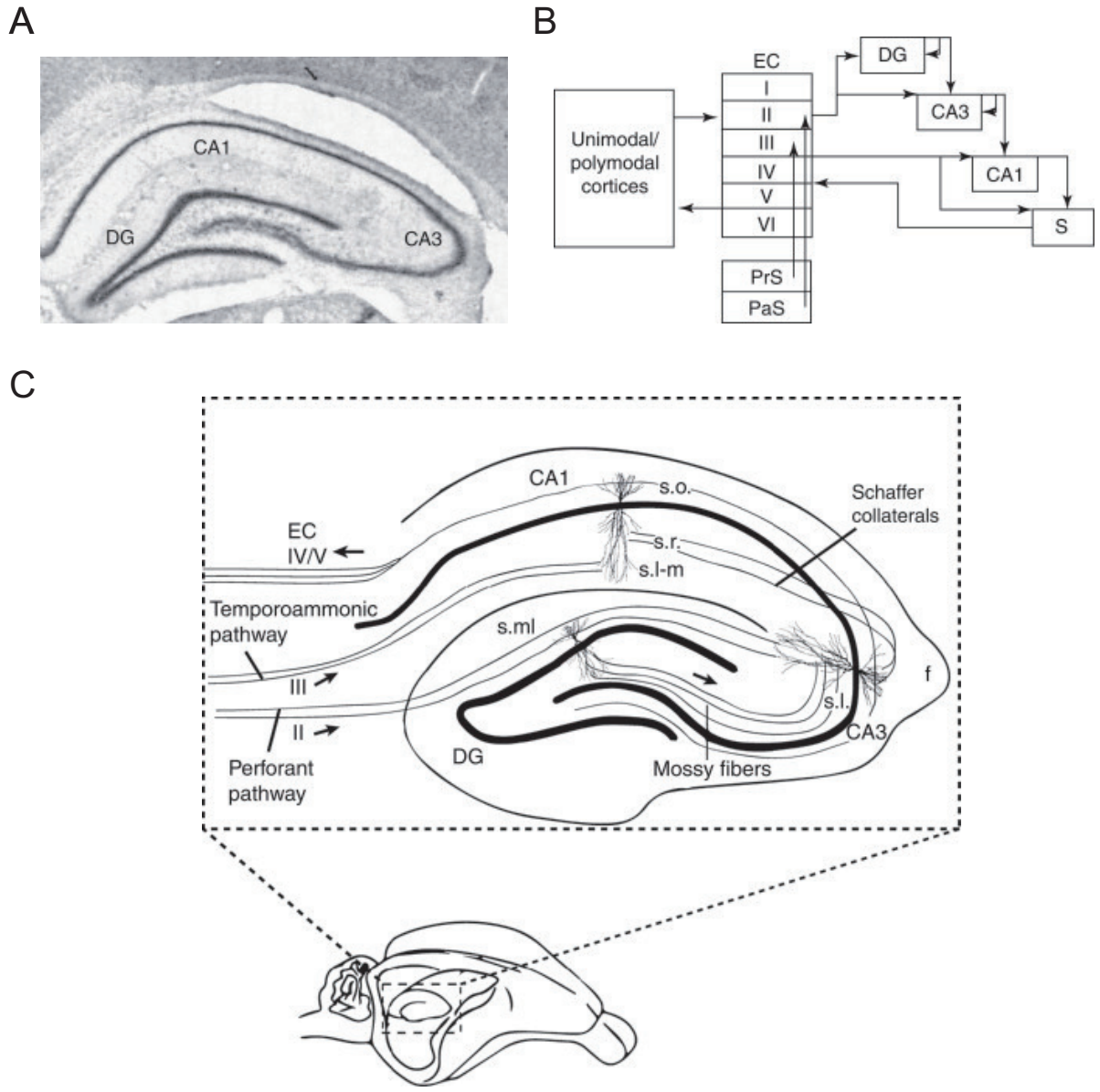

Figure 1.1: **Schematic diagram of a transverse slice through the hippocampus.**.

Figure 1.1 (continued): **Schematic diagram of a transverse slice through the hippocampus.**
A. A Nissl-stained transverse section through the rat hippocampal formation. The dark portions represent stained cell bodies in the dentate gyrus (DG) and cornu ammonis (CA) fields
B. A simplified circuit diagram showing the trisynaptic loop and additional connections. CA1, CA3, cornu ammonis fields; DG, dentate gyrus; EC, entorhinal cortex; PaS, parasubiculum; PrS, presubiculum; S, subiculum.
C. Schematic diagram of a transverse slice through the hippocampus showing the input of the entorhinal cortex (EC), to the DG fields, CA3, and CA1. Each of the primary fields can be further subdivided into strata. The apical dendrites of DG granule cells extend into stratum moleculare (s.ml). The apical dendrites of CA3 and CA1 pyramidal cells extend into stratum lacunosum-moleculare (s.l-m), stratum radiatum (s.r), and stratum lucidum (s.l; CA3 only), whereas the basal dendrites extend into stratum oriens (s.o.). The fornix (f) is a bundle of fibers that carry information from the hippocampus to the hypothalamus.
Figures and descriptions are adapted from Vago et al. (2017)

Within the hippocampal cell population, there are subsets of cells known as place cells, which exhibit spatial activity patterns corresponding to the animal's location within a specific environment (O'Keefe and Dostrovsky, 1971). These locations are referred to as place fields (PFs), and as a population they provide a spatial representation, or cognitive map, of a given environment (Wilson and McNaughton, 1993).

This spatial representation forms when an animal is introduced to a novel environment (Frank et al., 2004). Individual PFs in CA1 and CA3 form either instantly or after a delay in (Sheffield and Dombeck, 2019; Dong et al., 2021). Orthogonal place cell ensembles are involved in spatially representing different environments (Leutgeb et al., 2005). Once formed, hippocampal spatial representations stabilize with time and experience (Frank et al., 2004; Sheffield et al., 2017) and reactivate when the animal is re-introduced to the same environment (Frank et al., 2004). However, it has recently been discovered that these spatial representations may not be as stable as once thought. Even when animals

are navigating the same environment, evidence now suggests that spatial representations drift across time and experience (Ziv et al., 2013; Driscoll et al., 2022; Lee et al., 2020; Hainmueller and Bartos, 2018; Keinath et al., 2022; Dong et al., 2021; Mau et al., 2020), across new learning (Levy and Hasselmo, 2023), across reward contingencies (Krishnan et al., 2022). and following fearful experiences (Moita et al., 2004; Schuette et al., 2020; Ratigan et al., 2023). Rather than an issue with the system, drift has been proposed to be process in which the hippocampus continually learns, by updating representations over time and experience in an ever changing world. This is exactly what is expected of a memory system. However, the mechanisms of representational drift, and its association to continual learning, is yet to be fully understood. Drift will be further explored in chapter 2, with an investigation into the neural and experiential factors that influence it.

1.2 Role of hippocampal replay

Another line of evidence supporting the hippocampus' role in memory is the phenomenon of place cell sequence replay (Carr et al., 2011). It has been shown that place cell sequences activated during navigation are replayed at rest and during sleep, and may be a neural correlate of memory retrieval and/or consolidation (Wilson and McNaughton, 1994; Skaggs and McNaughton, 1996; Foster and Wilson, 2006; Diba and Buzsáki, 2007). Replay events can reactivate the PF sequence either forward or reverse in time, and may serve distinct functions. Disrupting hippocampal replay leads to impairment of spatial memory performance (Gridchyn et al., 2020) and impairment of learning (Igata et al., 2021). In Gillespie et al. (2021), replays were shown to be enriched for representations of previously rewarded locations. Together these studies indicate that replays play an important role in consolidating memory, and the salience of experience, i.e., rewarding experiences, are prioritized into memory through their increased replay.

Replays do not only represent past experience (Ólafsdóttir et al., 2018), but can also construct never-experienced novel-path sequences (Gupta et al., 2010). Place cells can construct reward related trajectories through visible yet inaccessible space (Ólafsdóttir et al., 2015), never-experienced optimized path (Igata et al., 2021), or 'preplay' future trajectories (Dragoi and Tonegawa, 2011). Also, it is shown (Diba and Buzsáki, 2007) that there are more forward replay events at the end of a run, reinstating the immediate past experience in the same sequence (suggesting memory consolidation) and more reverse replay events before navigation, associated with planning for future trajectories (suggesting retrieval of memory of the track). It is also shown that awake replays contribute to choices in memory guided tasks (Singer et al., 2013), which indicates how replays are associated with future planning. These studies expand on the potential function of replay events and also implicate neural dynamics in the hippocampus beyond memory processing, revealing a potential role in decision making and planning.

As hinted to above, replay events are not simply recapitulations of all experiences equally, but are instead modulated by the saliency of experience. Replay, in particular reverse replay, is shown to be more frequent for novel environments than familiar environments (Foster and Wilson, 2006). Rate and fidelity of the replays are shown to be modulated by difference in rewards (Singer and Frank, 2009). Also, replays of spatial trajectories associated with fear occur more than neutral trajectories (Wu et al., 2017). Replay events involved sequences associated with the zone where aversive experiences occurred, even though the animals did not enter the zone during the session (as they learnt to avoid the zone due to previous aversive experience). This indicates that the replay events participate in animals' avoidance of the dangerous zone and retrieval of the learned fear experience. Replays are also flexible (Widloski and Foster, 2022). When different configurations of barriers were introduced to

a familiar environment, replay events rapidly reflected the change in barrier configuration, without remapping of place fields. In Igata et al. (2021), it was observed that replays encoding paths towards novel/updated reward locations are more frequent than those encoding paths towards familiar rewarded locations. These studies show the role of replay in memory processing of salient experiences and their ability to update to support continual learning.

An intriguing observation of replays suggests they may support very rapid forms of learning that require only a single experience. Rapid one-shot learning is a feature of the hippocampus, and replay events have been shown to appear after a single experience of a novel environment (Berners-Lee et al., 2022). Replays then 'slow down' with repeated experience of the environment, by encoding greater details. This evolution of replay with familiarization with an environment shows that they likely participate in the initial encoding and then subsequent consolidation of spatial memories. Association of replay and learning is also shown in (Zheng et al., 2021) where they found that replays are more temporally compressed for correct trials and less compressed for error trials in a spatial memory task. The replay rate for the correct trial was also higher during rest. Intriguingly, an association with replay and observational learning has also been shown Mou et al. (2022). Animals learned a T-maze tasks by observing a demonstrator's spatial trajectories, and remote replay events were observed in the observer's hippocampus, preferring reward sites and predicting future trajectories. When there was no demonstrator, such predictive power disappeared.

In this thesis, I will investigate the cellular and experiential factors that influence representation drift and replay events in CA1. The observations will provide insight into the underlying mechanisms that drive these memory related neural dynamics in the hippocampus.

CHAPTER 2

THE PRECISION OF PLACE FIELDS GOVERNS THEIR FATE ACROSS EPOCHS OF EXPERIENCE

2.1 Introduction

As introduced in Introduction, reactivation of hippocampal representations is believed to support memory retrieval. However, as described in Introduction, recent findings show that spatial representations change with time and experience even when animals are navigating the same environment (Driscoll et al., 2022; Lee et al., 2020; Hainmueller and Bartos, 2018; Keinath et al., 2022; Dong et al., 2021; Mau et al., 2020). This phenomenon is known as representational drift and can occur during navigation of an environment from lap-to-lap, as demonstrated by many PFs shifting backwards (Dong et al., 2021; Roth et al., 2012a; Mehta et al., 2000), and across repeated exposures (epochs of experience) to the same environment on different days (Ziv et al., 2013; Dong et al., 2021). Representational drift may track time (Mankin et al., 2012; Rubin et al., 2015; Mankin et al., 2015) or amount of experience (Khatib et al., 2023; Geva et al., 2023). Similar changes to the spatial code are observed when animal's undergo an internal state change during navigation, as demonstrated when attention or reward expectation is altered in an unchanging spatial environment (Krishnan et al., 2022; Pettit et al., 2022). At the single cell level, the fate of pre-existing place fields falls into one of 3 categories. First, place cells can remap their PFs to new locations. Second, PFs can vanish. Third, place fields can remain stable. However, what determines the fate of PFs across time or internal state changes remains unclear.

To investigate this, we reanalyzed previously published data, where 2-photon Ca^{2+} imaging was used to record the activity of large populations of pyramidal neurons in dorsal CA1 in head-fixed mice. Mice were placed on a treadmill and repeatedly traversed a virtual linear environment for water rewards. We defined cells with significant PFs during a block of trials

in a single session and measured their lap-to-lap properties such as their spatial precision, firing rate variability, and backward shifting. We then determined PF fate in the same environment in either a subsequent block of trials separated by a day (a distinct temporal epoch) or a subsequent block of trials during the same session but with reward removed to change reward expectation (a distinct internal state epoch). Our findings reveal that remapped PFs across internal state or temporal epochs tended to have lower spatial precision during the initial epoch, whereas stable and vanished PFs were associated with high spatial precision. This suggests that place cells with imprecise place fields generally possess greater spatial flexibility, providing a means for the hippocampus to respond to distinct epochs of experience and update spatial representations with new spatial information. Place cells with precise place fields, when they reappear, generally retain the same spatial information about the environment across epochs.

2.2 Materials and Methods

2.2.1 Subjects

All experimental and surgical procedures were in accordance with the Animal Care and Use Committee guidelines of authors' institution. For this study, 10-12-week-old male C57BL/6J wildtype (WT) mice (23-33g) were individually housed in a reverse 12 h light/dark cycle with an ambient temperature of ∼20 °C and ∼50% humidity. Male mice were used over female mice due to the size and weight of the headplates (9.1 mm × 31.7 mm, ∼2g), which were difficult to firmly attach to smaller female skulls. All training and experiments were conducted during the animal's dark cycle.

2.2.2 Mouse surgery and virus injection

Mice were anesthetized (∼1-2% isoflurane) and injected with 0.5 mL of saline (intraperitoneal injection) and ∼0.45 mL of meloxicam (1–2 mg/kg, subcutaneous injection). For CA1 population imaging, a small (∼0.5-1.0 mm) craniotomy was made over the hippocampus CA1 (1.7 mm lateral, -2.3 mm caudal of Bregma). A genetically encoded calcium indicator, AAV1-CamKII-GCaMP6f (Addgene, #100834) was injected into CA1 (∼75 nl) at a depth of 1.25 mm below the surface of the dura using a beveled glass micropipette. Afterwards, the site was covered up using dental cement (Metabond, Parkell Corporation) and a metal head-plate (9.1 mm × 31.7 mm, Atlas Tool and Die Works) was also attached to the skull with the cement. Mice were separated into individual cages and water restriction began the following day (0.8–1.0 ml per day). Around 7 days later, mice underwent another surgery to implant a hippocampal window as previously described (Dombeck et al., 2010). Following implantation, the head plate was reattached with the addition of a head ring cemented on top of the head plate which was used to house the microscope objective and block out ambient light. Post-surgery, mice were given 2-3 ml of water/day for 3 days to enhance recovery before returning to the reduced water schedule (0.8-1.0 ml/day).

2.2.3 Behaviour and Calcium imaging

We analyzed previously published data.

For the experiment across days (Dong et al., 2021), mice (n = 5 in total) were trained to run on a treadmill along a 3 m VR linear track with 4 um of water reward delivered at the end of the track (the familiar environment (F)). Mice (n = 3, #1, 2, 3) were then imaged over two days in the same environment , without exposure to any novel environment. Calcium activity in CA1 pyramidal neurons (n = 1282 neurons) were extracted using customized MATLAB script (Sheffield et al., 2017), with parameters and procedures detailed in Dong

et al. (2021).

For the experiment involving the novel environment (N) switch, mice were trained to run on a treadmill in F, and then on imaging days, the mice (n = 3, #3, 4, 5) were introduced to N with different 3D visual cues but the same reward location and track length as F. Note that this novel environment N is N2 in Dong et al. (2021). Also note that mouse #3 was also imaged for the experiment in the familiar environment. Again, calcium activity of CA1 pyramidal neurons (n = 1704 neurons) were extracted with the same approach. Table 2.1 lists the experimental conditions each animal went through and how they were included in Dong et al. (2021)

For multi-day imaging datasets, we take an average image at the end of the imaging session on day1 and use it as a template to find the exact same FOV the following day in real-time (i.e. before we start collecting data on that day). We match the FOVs within 1um of z-plane alignment (that is the limit of our microscope controller). We further check alignment by concatenating the FOVs across days and motion correcting them together as one single time-series movie. This corrects for any differences in X and Y position and allows us to closely inspect any z-differences at the frame transition from day1 to day2. If movies from different days are rotated relative to one another, Fiji (ImageJ) is used to correct any rotational displacement between the two movies. We do not use any FOVs that have any noticeable differences in z-planes at the transition. All the data shown in this paper are matched in X, Y, and Z. Example of FOVs across days can be found in Fig.2.1B. ROIs are extracted after concatenation. To rule out that the results are not due to imaging artifacts, Fig 2.7 shows that there is no correlation between anatomical location of place cells in the FOV and their PF fate. If any imaging artifacts were affecting our PF measurements, the 3 categories would be equally affected.

Table 2.1: Subjects

Subject #	Imaging sessions	Familiar - 2 days (before any exposure to novelty)	Novelty - 2 days (N2 in Dong et al. (2021))	Included in Dong et al. (2021)?
1	Training: F (imaged) Day 1: F (imaged)	✓	×	Not included. Only imaged in F
2	Training: F (imaged) Day 1: F, N1 (imaged)	✓	×	Included for analysis of F vs N
3	Training: F (imaged) Day 1: F, N1(imaged) Day 2: F, N2 (imaged) Day 3: N2(imaged)	✓	✓	Included for analysis of F vs N and also re-exposure to N2
4	Training: F (NOT imaged) Day 1: F, N1(imaged) Day 2: F, N2 (imaged) Day 3: N2(imaged)	×	✓	Included for analysis of F vs N and also re-exposure to N2

Continued on next page

Table 2.1: Subjects (Continued)

Subject #	Imaging sessions	Familiar - 2 days (before any exposure to novelty)	Novelty - 2 days (N2 in Dong et al. (2021))	Included in Dong et al. (2021)?
5	Training: F (NOT imaged) Day 1: F, N1(imaged) Day 2: F, N2 (imaged) Day 3: N2(imaged)	×	✓	Included for analysis of F vs N and also re-exposure to N2

For the experiment with change in reward contingencies (Krishnan et al., 2022), mice were trained on a 2 m VR linear track for water reward. Well-trained mice showed pre-emptive licking before the reward location. On experimental day, the mice (n = 5) ran in the environment with reward (R), then the reward was unexpectedly removed (UR). The reward was then re-introduced (RR). Each condition (R, UR and RR) lasted 8-10 minutes. Population activity of CA1 pyramidal neurons (n = 1288) were measured with Ca^{2+} imaging, across the conditions. Calcium transients were extracted using suite2p (Pachitariu et al., 2017) as in Krishnan et al. (2022).

2.2.4 Defining PFs

After extracting significant calcium transients, we correlated the transients to the animals' behaviour. We obtained the significant peak of each transient by finding the local maximum of a transient that exceeds the mean $\Delta F/F$ by 3 inter-quartile range of $\Delta F/F$ in a time window of 20 frames, to avoid including peaks from noise. The corresponding animal location on the track were then obtained. Fluorescence peaks were treated as events in a

2-D parameter space (time and location). PFs were then defined by event clusters in the 2D parameter space using the clustering algorithm DBSCAN (Ester et al., 1996), a density based clustering algorithm. A cluster then needed to include events from at least 10 different laps to be considered a PF.

The vast majority of cells had either a single cluster or no cluster in any given epoch. In the limited number of cells that had multiple clusters in either epoch, each cluster was treated as independent PF. For the very few cells with multiple clusters in epoch 1 and epoch 2, the clusters across the epochs were "paired", such that clusters in epoch 1 were paired with the closet ones in epoch 2 and analyzed as such. In cases with two clusters in epoch 1 and one cluster in epoch 2, we considered the clusters to have merged across epochs If both clusters in the first epoch were within 40 cm of the epoch 2 cluster (if one or both were not, we did not consider them merged and treated each independently). The two clusters in epoch 1 were therefore counted as one stable PF and we combined their spatial precision values (see PF properties on how we did this), to avoid over-counting the stable PFs. This caused the difference in total number of PFs in R for Fig. 2.3C and Fig. 2.3D, due to cells with multiple clusters in R having different fates in UR and RR.

2.2.5 PF properties

Once clusters were identified as PFs, the time, location and transient peak $\Delta F/F$ for each event within the cluster were quantified. To determine the onset and offset of the PF, we defined the PF onset lap as the lap number of the first event in the cluster, and the PF offset lap as the lap number of the last event in the cluster. The duration of the PF was then calculated as the difference between the onset and offset lap.

The spatial location of the PF was defined as the median of the locations of the events within the cluster. The spatial precision of the PF was quantified using the standard deviation (SD) of the location in the cluster. Therefore, a precise PF means a lower lap-to-lap variation in

firing location, and hence a lower SD. To ensure that this measurement was not influenced by the edges of the track, PFs located within 10 cm of the track ends were excluded from the analysis.

In the rare cases where two PFs merged into a single PF across epochs (see Defining PFs), we combined their precision measure into a single value and only counted it as a single stable PF. To obtain a single precision value from the two PFs, we obtained the location of each event from each cluster and then subtracted the mean location of that cluster from each event ($x_i - \bar{x}$). Then, the two mean-removed sets of locations were merged and the spatial precision was measured by SD of the merged set. This was performed to determine the combined spatial precision of the two PFs, that we considered a single stable PF for this analysis.

The PF firing rate dynamics were investigated by using the $\Delta F/F$ peak amplitude as a proxy for the maximum firing rate. The lap-by-lap firing rate dynamics were measured by calculating the deviation in the peak amplitude of events within the cluster.

2.2.6 PF categorization

To assess the spatial stability of PFs, we categorized them based on their change in spatial location across days/conditions.

1. Stable - The PF is present on both days/conditions and any change in PF position is: $\Delta < 40$ cm
2. Remapped - The PF is present on both days/conditions but changes PF position: $\Delta > 40$ cm
3. Vanished - The PF is only present on the first day/condition

The specific choice of 40 cm as the threshold was made to ensure that it was larger than the typical fluctuation observed in peak locations within clusters in the dataset (a measure of PF width). This means that a change in location beyond 40 cm would typically mean a

non-overlapping PF.

2.2.7 PF backward shifting

PFs were aligned by their onset lap, which was defined as the lap number of the first peak in that cluster. Then the spatial positions of the PFs on each lap were obtained with a sliding window of 5 laps. The 5-lap sliding average position of individual PFs were then compared to the median location calculated from laps beyond the 15th lap from the onset lap for that PF. For each lap from the PF onset lap, the average shift over the population of PFs was calculated and plotted. An exponential fit (least square fit, scipy.optimize.curve_fit) was then applied to the trend. The error of the fitting parameters were obtained by the square-root of the diagonal elements of the covariance matrix (returned by curve_fit). The same trend was observed without the smoothing.

PFs were considered to have ceased systematically backward shifting after $2T$ laps from their onset, as the decay in shift is reduced to $e^{-2} = 13.5\%$ at $2T$. Peaks after $2T$ laps were included in the comparisons that restrict to PF activity following backward shifting. Similar trends were observed using different choices than $2T$ for the cutoff.

2.2.8 Statistics

For the plots regarding PF backward shifting, the error bars represent mean ± SEM.

To generate the plots comparing the spatial precision, we used the package DABEST ('data analysis with bootstrap-coupled estimation') (Ho et al., 2019). As explained in PF properties, this gives a measure of the precision of PFs in each category. To compare the difference in the population, the median difference between the distributions and its confidence level were obtained with bootstrapping (5000 re-samples). P-values of the non-parametric two-sided approximate permutation t-test were reported.

Schematic figures (Fig. 2.1A, Fig. 2.2A, Fig. 2.3A) were created with BioRender.com

2.3 Results

2.3.1 Place fields that remap across two days in a familiar environment have lower spatial precision on day 1

To address whether place field characteristics during a single epoch of navigation in an environment were associated with their fate during a second epoch of the environment, head-fixed mice (n = 3) were trained to navigate a familiar VR environment (Fig. 2.1A) while the same populations of place cells were imaged in CA1 during 2 blocks of trials (distinct temporal epochs) separated by a day (Fig. 2.1B). The peak Ca^{2+} fluorescence on each lap traversal was used as a proxy for maximum spatial firing position on each lap. Peaks were then treated as events in 2D parameter space (time and spatial position). Clusters of events with consistent spatial position were identified as PFs (see Materials and Methods). The mean spatial position was then calculated and the same analysis was done the following day. PFs calculated on day 1 were then defined as either stable, remapped, or vanished based on their mean activity on day 2 (see PF categorization and Fig. 2.4). PFs were considered remapped if the change in PF location across days was greater than 40 cm (see Methods for why this threshold was chosen). Note that in this paper we distinguish between PFs that change spatial position (referred as 'remapped') and PFs that disappear (referred as 'vanished') (see examples Fig. 2.1D). The median change in spatial position across days in the stable PF group was 2.6 cm versus 179.8 cm in the remapped group (Fig. 2.4A).

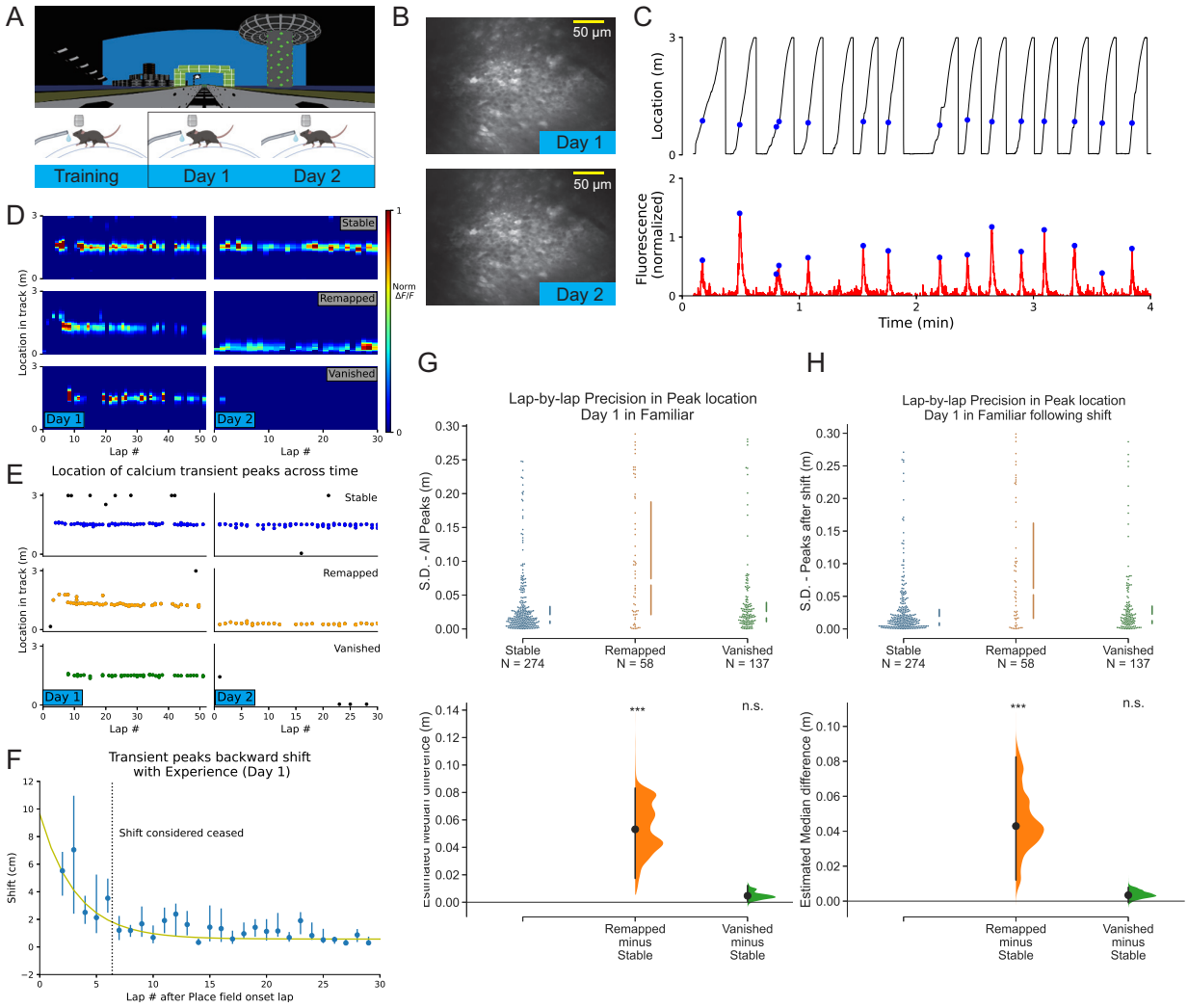

Figure 2.1: **Place fields that remap across two days in a familiar environment have lower spatial precision on day 1.**

Figure 2.1 (continued): **Place fields that remap across two days in a familiar environment have lower spatial precision on day 1**.
(A) Experimental design. Top: the familiar virtual reality (VR) environment. Bottom: Animals trained and recorded in the same VR environment.
(B) Example field of view showing imaging of the same cells on Day 1 and 2.
(C) Top: Behavior of a single animal showing track location. Blue dots indicate Ca^{2+} fluorescence peaks from an example cell relative to the animal's track location. Bottom: Fluorescence trace of the example cell across time. Blue dots indicating the peak of the Fluorescence change.
(D) Examples of Stable, Remapped and Vanished place fields across days. Bins near ends of track are excluded.
(E) Same as (D), but place fields are identified by transient peaks. Coloured (blue, orange and green) dots indicate in-field fluorescence peaks. Black dots are out of field peaks.
(F) Average population backward shift of PF peaks on day 1. PFs are aligned to their onset lap. Line indicates fitted exponential curve: $F(x) = Ae^{-x/T}$, with $A = 9.1 \pm 4.3$ cm, $T = 3.2 \pm 1.1$ laps
(G) Comparison of spatial precision of PFs (469 PFs in day 1) from the 3 categories by measuring the standard deviation of the lap-by-lap peak locations of Stable (274/469; 58.4%), Remapped (58/469; 12.4%) and Vanished (137/469; 29.2%) PFs. Bottom: bootstrapped median difference between the three groups. 5000 re-samples, ***P = 4.135E-07 for Remapped vs Stable, P = 0.140 for Vanished vs Stable
(H) Same as (G), but includes only peaks after backward shifting. 5000 re-samples, ***P = 2.641E-13 for Remapped vs Stable, P = 0.248 for Vanished vs Stable.

Various properties of individual PFs in each category were then analyzed on day 1. First, lap-wise spatial precision was quantified using the standard deviation (SD) of spatial locations of the fluorescent peaks. We compared the spatial precision of PFs across the 3 categories (Fig. 2.1F). The PFs that remapped on day 2 exhibited significantly lower spatial precision on day 1, as revealed by a higher variation in lap-to-lap PF position (Mdn SD = 6.9 cm, IQR = 2.1 - 18.8 cm) than stable PFs (Mdn SD = 1.6 cm, IQR = 0.8 - 3.3 cm; P = 4.135E-07). Vanished PFs, however, exhibited similar spatial precision to stable PFs (Mdn SD = 2.2 cm, IQR = 1.1 - 3.9 cm; P = 0.14).

Studies have reported a type of drift on a lap-by-lap basis that occurs during navigation - also known as PF backward shifting (Dong et al., 2021; Khatib et al., 2023; Geva et al., 2023; Mehta et al., 2000; Lee and Knierim, 2007; Roth et al., 2012a). Backward shifting could reduce the lap-wise precision of PFs as we measured it here. To determine whether backward shifting contributed to our measure of precision and its association with PF fate, we measured the extent of backward shifting on day 1 (Fig. 2.1E). Further, because not all PFs emerge immediately when mice start navigating a familiar environment on any particular day, we first defined the PF onset lap for each PF (Sheffield et al., 2017; Dong et al., 2021). Aligning PFs to their onset lap, we found that backward shifting ceased after a finite number of laps, and the decay of shifting could be well fitted to an exponential (Fig. 2.1E). We estimated the time constant T of the decay. We considered PFs to have ceased backward shifting after $2T$ laps from their onset, as this is the point at which 90% of the shifting had decayed (see PF backward shifting). Then, the same comparison was performed as Fig. 2.1F, but restricted to PF activity following the backward shifting. We found that the association between PF precision and PF fate across days was maintained even when backward shifting on day 1 was excluded from the analysis Fig. 2.1G. (Stable PFs: Mdn SD = 1.4 cm, IQR = 0.5 - 3.0 cm; Remapped PFs: Mdn SD = 5.7 cm, IQR = 1.6 - 16.2 cm; Vanished PFs: Mdn SD = 1.7 cm, IQR = 0.8 - 3.5 cm). This was also true for individual animals, shown in Fig. 2.6A.

It is possible that cells closer to the center of the imaging field of view (FOV) are of higher image quality, i.e., are less sensitive to imaging artifacts which could introduce noise. Cells further from the center of the FOV could therefore produce noisier signals that could make their PFs appear less precise and also make them more difficult to detect across days, making them appear less stable. To test whether this potential artifact is driving the association between PF precision and PF fate, we correlated the anatomical location of place cells in the FOV with their PF fate, which is shown in Fig 2.7 for three example animals. We found no correlation between the location of place cells in the FOV and the fate of their PFs across days, ruling out any imaging artifacts driving the association between PF precision and fate.
We next checked if the remapped and stable PFs continued to have differences in spatial precision on day 2 (Fig. 2.5A). We found no such difference, showing that on day 2, the PFs that had remapped and the PFs that had stabilized have the same median precision. This suggests that PFs can switch from one category to the other. In other words, an imprecise PF that remaps across a day can then become precise and therefore stable across a subsequent day, and vice versa. While the spatial precision on day 1 is relevant to PF fate across a day, we next tested if other PF properties on day 1 were associated with PF fate. We first asked if the extent of backward shifting of PFs was associated with their fate. In Fig. 2.8A, we show the lap-by-lap shifting of all the PFs, and separately, the PFs from each category fitted to an exponential. Remapped, stable, and vanished PFs showed similar backward shifting dynamics. Comparing both the amplitudes and the time constants for the exponential fits along with their uncertainty values for all the categories demonstrated no differences between the groups (Fig. 2.8A).
Next, we asked if PF firing rates were associated with PF fate. Using peak amplitudes of calcium transients as a proxy for max firing rate on each PF traversal, we quantified the median and deviation in amplitudes from lap-to-lap. Comparing this measure between the 3 categories of PF fate revealed no significant difference (Fig. 2.8B,C).

Not only do PFs emerge on different laps in a familiar environment, place cells can stop firing in their PF before the session ends. The PF onset lap and PF end lap, as well as the total laps in between onset and end (PF duration), can therefore be quantified for each PF. Fig. 2.8D shows the histograms of PF onset laps, end laps and total laps for the three PF fate categories. We found no differences between the PF fate categories.

Together, our investigation into place field properties and PF fate across days in a familiar environment suggests that it is randomly varying lap-by-lap spatial dynamics on day 1 that is related to the across-day fate of PFs, and other PF properties are unrelated.

2.3.2 Place fields that remap across two days in a novel environment have lower spatial precision on day 1

When mice are introduced to a novel environment, global remapping occurs in CA1 in which a new map forms (Colgin et al., 2008; Sheffield et al., 2017; Dong et al., 2021). Once the PFs that comprise the new map emerge, they typically are less precise than in familiar environments (Frank et al., 2004). We therefore tested if the relationship between lap-wise precision and across-day PF fate that we observed in a familiar environment also occurred in a novel environment during familiarization. We therefore switched mice (n = 3) to a novel VR environment while imaging CA1 (Fig. 2.2A-B) and identified PFs (Fig. 2.2C). We first wanted to determine how the newly-formed PF map backward shifted from lap-to-lap on day 1 (Fig. 2.2D). We found backward shifting was prolonged compared to the familiar environment ($T = 3.2 \pm 1.1$ laps for familiar environment and $T = 5.3 \pm 1.0$ laps for novel environment) as previously reported (Dong et al., 2021). We then measured PF precision on day 1 and compared between the three categories of PFs based on their fate on day 2. Once again, we observed that remapped PFs had lower spatial precision than stable and vanished PFs as shown by having a higher median SD (Fig. 2.2F; Remapped PFs: Mdn SD = 5.4 cm, IQR = 2.8 - 8.4 cm; Stable PFs: Mdn SD = 3.4 cm, IQR = 1.7 - 6.1 cm; ; Vanished PFs:

Mdn SD = 3.2 cm, IQR = 1.7 - 6.5 cm), even when backward shifting was excluded from the precision analysis (Fig. 2.2G; Remapped PFs: Mdn SD = 3.8 cm, IQR = 2.1 - 6.9 cm; Stable PFs: Mdn SD = 2.7 cm, IQR = 1.1 - 4.9 cm; Vanished PFs: Mdn SD = 2.7 cm, IQR = 1.3 - 5.3 cm). Also, just as in a familiar environment, day 2 lap-by-lap precision showed no difference between remapped and stable PFs (Fig. 2.5B), and no other PF properties measured on day 1 were related to PF fate on day 2 (Fig. 2.9).

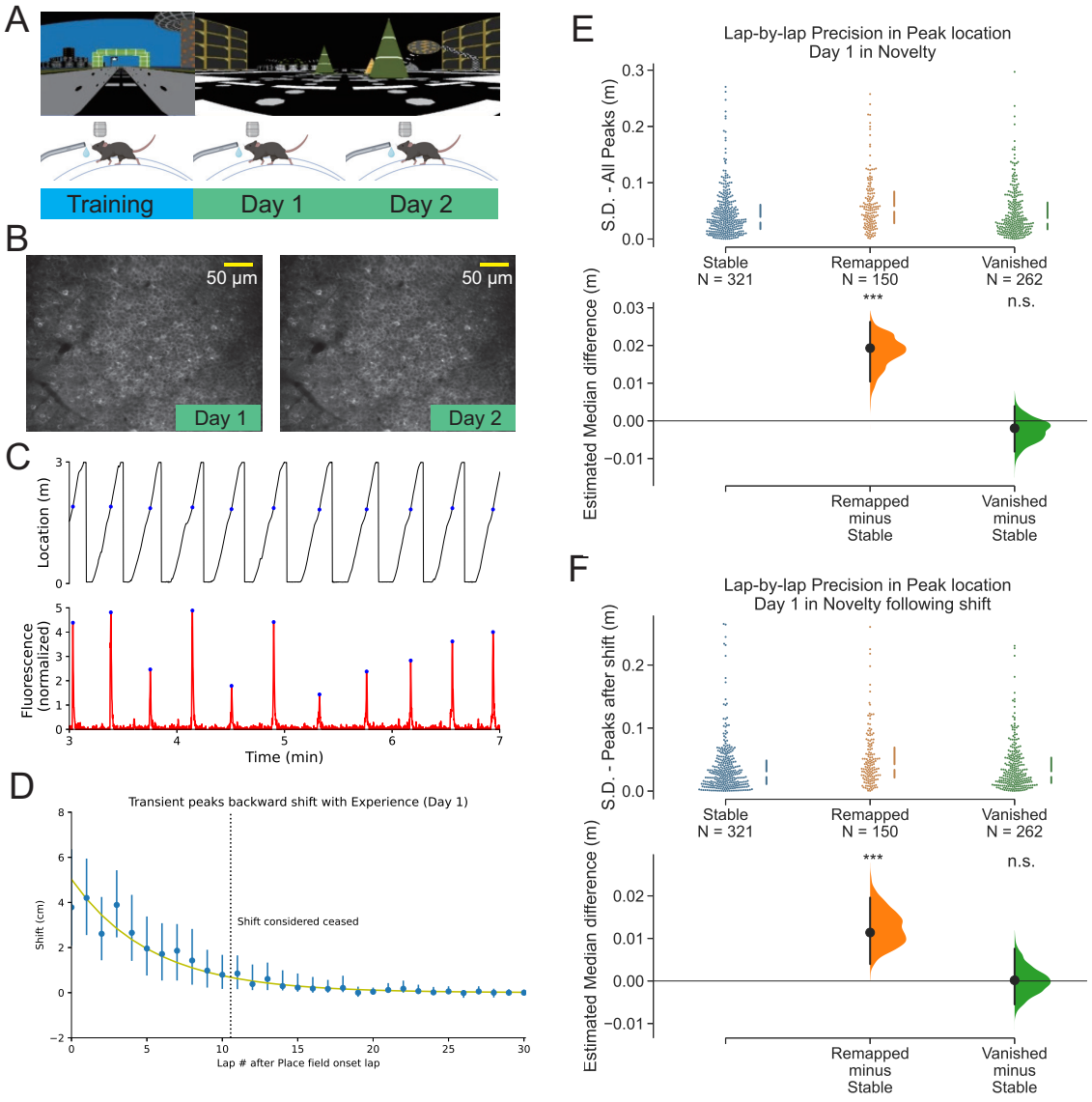

Figure 2.2: **Place fields that remap across two days in a novel environment have lower spatial precision on day 1.**

Figure 2.2 (continued): **Place fields that remap across two days in a novel environment have lower spatial precision on day 1**
(A) Experimental design. Top: the familiar environment (F) and the novel environment (N). Bottom: The animals were trained in a familiar environment, then switched to a novel environment and imaged for two days.
(B) Example field of view for Day 1 and 2 showing the same imaged cells.
(C) Top: Behaviour of a single animal showing track location. Blue dots indicate the animals location when the example cell's calcium transient is at its peak. Bottom: Time-series fluorescent trace for an example cell. Blue dots indicating the transient peaks.
(D) Average population backward shifting of PF peaks within the session on day 1. PFs are aligned to their onset lap. Line indicates fitted exponential curve: $F(x) = Ae^{-x/T}$, with $A = 5.0 \pm 1.3$ cm, $T = 5.3 \pm 1.0$ laps
(E) Comparison of spatial precision of PFs (733 PFs on day 1) from the 3 categories by measuring the standard deviation of the lap-by-lap peak locations of Stable (321/733, 43.8%), Remapped (150/733, 20.5%) and Vanished (262/733, 35.7%) PFs. Bottom: bootstrapped median difference between the three groups. 5000 re-samples, ***P = 1.833E-05 for Remapped vs Stable, P = 0.383 for Vanished vs Stable.
(F) Same as (E), but includes only peaks after the backward shifting. 5000 re-samples, ***P = 0.0006 for Remapped vs Stable, P = 0.959 for Vanished vs Stable.

2.3.3 Place fields that remap in response to changed reward expectation tend to have lower spatial precision before the change

A recent study showed that some PFs remap when the internal state of reward expectation changes in an unchanging spatial environment (Krishnan et al., 2022). We therefore asked whether lap-by-lap spatial precision of PFs was associated with remapping under these conditions of altered internal state. To do this, mice were trained and then imaged in the same familiar rewarded environment (Fig. 2.3A). Trained mice (n = 5) were first water rewarded for a block of trials and then reward was removed for a subsequent block of trials (Unrewarded condition: UR). After a few laps, mice stopped pre-emptively licking for reward, demonstrating a loss of reward expectation (Krishnan et al., 2022). Then, reward was reintroduced (Re-rewarded condition: RR).

Fig. 2.3B shows example place cells; one with a stable PF across the R-UR-RR conditions (top), one with a remapped PF across all conditions (middle), and one PF that vanished in UR but reappeared in RR (bottom). We then investigated whether the lap-by-lap spatial precision of PFs in R determined their fate in UR or RR (Fig. 2.3C, D). Similar to the fate of PFs across days, we found that the remapped PFs in UR exhibited lower spatial precision in R (Fig. 2.3C; Remapped PFs: Mdn SD = 1.9 cm, IQR = 1.2 - 3.0 cm; Stable PFs: Mdn SD = 1.4 cm, IQR = 0.8 - 2.2 cm; Vanished PFs: Mdn SD = 1.3 cm, IQR = 0.4 - 2.1 cm) and RR (Fig. 2.3D; Remapped PFs: Mdn SD = 2.0 cm, IQR = 1.2 - 3.4 cm; Stable PFs: Mdn SD = 1.3 cm, IQR = 0.8 - 2.2 cm; Vanished PFs: Mdn SD = 1.2 cm, IQR = 0.5 - 1.9 cm) . Again, other PF properties had no association with remapping or stability (Fig. 2.10 and Fig. 2.11). This indicates that across the population, remapped PFs caused by internal state changes tend to have lower precision than stable/vanished PFs, behaving similarly to remapped PFs across days.

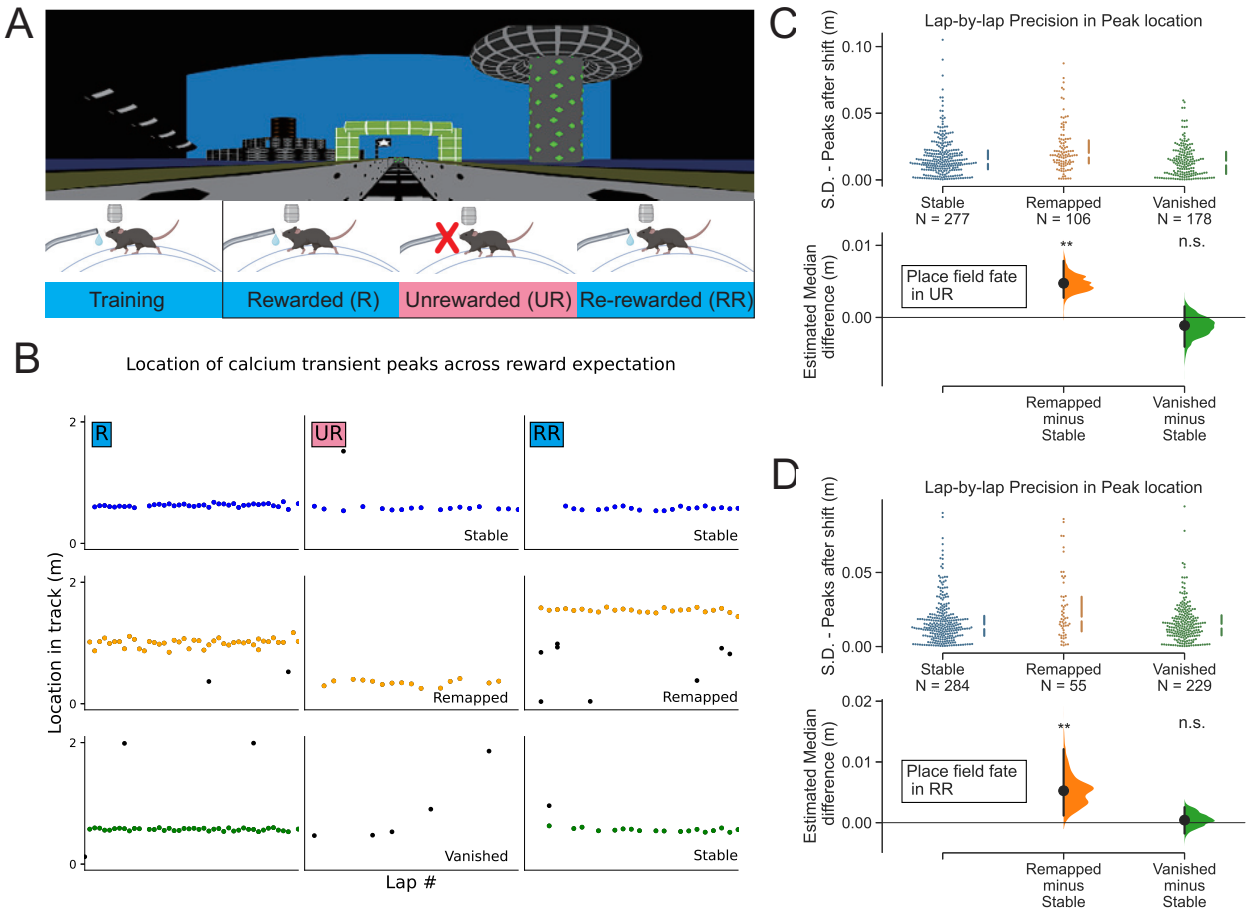

Figure 2.3: **Place fields that remap in response to changed reward expectation tend to have lower spatial precision before the change**.
(A) Experimental design. Top: the familiar VR environment. Bottom: The Animals were trained and recorded in the same VR environment during changes in reward.
(B) Example of stable (top), remapped (middle) and vanished (bottom) place fields across changes in reward expectation. Coloured (blue, orange and green) dots indicate in-field transient peaks. The place field can undergo remapping in UR and then again in RR.
(C) Comparison of spatial precision of PFs (561 PFs in R, see Defining PFs) from the 3 categories by measuring the standard deviation of the lap-by-lap peak locations of stable (277/561, 49.4%), remapped (106/561, 18.9%) and vanished (178/561, 31.7%) PFs between R and UR. Bottom: bootstrapped median difference between the three groups. 5000 re-samples, **P = 0.0016 for remapped vs stable, P = 0.480 for vanished vs stable
(D) Same as (E), but comparison between R and RR. (568 PFs in R, see Defining PFs; Stable PFs: 284/568, 50.0%; Remapped PFs: 55/568, 9.7%; Vanished PFs: 229/568, 40.3%) 5000 re-samples, **P = 0.0022 for remapped vs stable, P = 0.683 for vanished vs stable

2.4 Discussion

We investigated hippocampal CA1 spatial code dynamics occurring across epochs in unchanging spatial environments to determine whether firing characteristics during a single epoch was associated with how cells encode future epochs. Our findings show that PFs that remapped across epochs separated in time by a day, or across epochs distinguished by differences in reward expectation, had a statistically lower lap-by-lap spatial precision during the initial epoch, compared to stable and vanished PFs. This held true across epochs in novel environments as mice underwent familiarization (a form of learning). Other lap-by-lap characteristics of PFs, such as firing rate variability, backward shifting dynamics, PF onset, PF offset, and PF duration were not associated with the fate of PFs across epochs. This indicates that the spatial firing precision of PFs during navigation is related to their tendency to remap or stabilize/vanish across distinct epochs of experience.

Drift across time has been observed in different parts of the brain (Deitch et al., 2021; Marks and Goard, 2021; Driscoll et al., 2017; Schoonover et al., 2021). In the hippocampus, an accurate representation of the spatial environment is preserved during drift (Ziv et al., 2013; Keinath et al., 2022), suggesting drift may encode non-spatial factors of the context such as time (Mankin et al., 2012, 2015), and experience (Khatib et al., 2023; Geva et al., 2023). Our data suggest that the dynamics of drift across epochs is related to the cellular activity within an epoch. This also holds true for epochs that are separated by internal state changes. The dynamics of the hippocampal spatial code across epochs may therefore not be random and may instead be predictable. However, the extent of predictability remains to be directly tested.

A possible explanation for the relationship between lap-by-lap dynamics and the tendency to remap is that those PFs with less spatial precision simply receive higher variability in the activation of the CA3 inputs they receive (Zutshi et al., 2022; Davoudi and Foster, 2019; Devalle

and Roxin, 2022). Alternatively, evidence suggests that all CA1 pyramidal cells may receive synaptic input regarding all locations in an environment from CA3 (Grienberger et al., 2017). What determines whether a cell fires at a given location may therefore be the strength of synapses activated at particular locations. Indeed, dendritic spikes in CA1 place cells, which is a reflection of strong synaptic input to a dendritic branch, is associated with PF stability across days (Sheffield and Dombeck, 2015). One idea is that these strong synapses may have undergone Hebbian potentiation, and together with the resultant somatic firing may induce homeostatic mechanisms that lower overall cellular excitability (through synaptic or intrinsic excitability renormalization) (Miller, 1996) and make other sets of synapses too weak to cause somatic firing in a winner-takes-all manner (Sheffield and Dombeck, 2015; Barry and Burgess, 2007). This process would result in a precise PF as the cell would fire only in response to those specific inputs. The dendritic spikes associated with this strong input may further serve to maintain synaptic strength to stabilize the PF across days (Sheffield and Dombeck, 2015). On the other hand, PFs with more lap-wise fluctuations in spatial firing may reflect differences in the sets of synapses activated from lap-to-lap. Such variations may not engage Hebbian potentiation and thus avoid the homeostatic winner-takes-all process described above. This would both cause the cell to be less precise from lap-to-lap but also allow the cell more flexibility to respond to new sets of synaptic activation that may occur across distinct epochs of experience, allowing for continuous encoding of new information in the hippocampus.

Our results also show that the PFs that vanished across epochs are indistinguishable from the stable ones in terms of spatial precision. This aligns with previous literature (Ziv et al., 2013), that place cells enter and exit an active subset of an underlying stable map. When these cells are active again, their PFs retain their locations (Ziv et al., 2013). The PFs that vanished across epochs may actually be part of this stable map, they are just not participating in the active subset during a particular epoch. This is likely due to the CA3 inputs

that could drive them to fire not being activated.

Overall, our study presents how lap-by-lap dynamics of PFs during an epoch of experience relate to spatial code dynamics across epochs in the same environment. This work provides insight into why some cells remap and others remain stable/vanish. It also provides insight into the synaptic mechanisms which may facilitate these cellular dynamics to support episodic memory encoding.

2.5 Supplementary Material

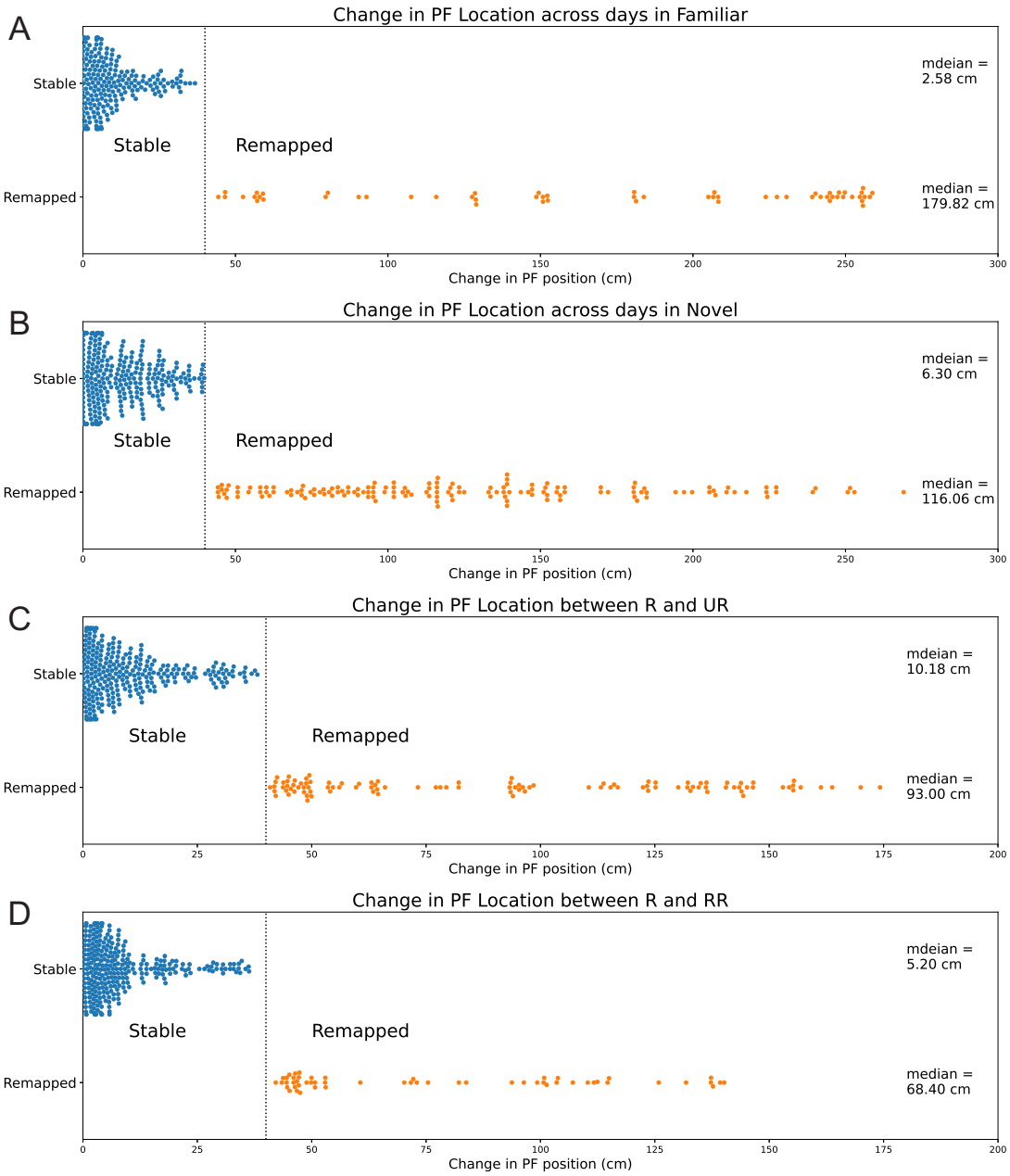

Figure 2.4: **Change in PF locations between blocks of trials**

Figure 2.4 (continued): **Change in PF locations between blocks of trials**
(A) Change in PF locations across days in the familiar environment. Median of each category shown in figure.
(B) Change in PF locations across days in the novel environment. Median of each category shown in figure.
(C) Change in PF locations between R and UR. Median of each category shown in figure.
(D) Change in PF locations between R and RR. Median of each category shown in figure.

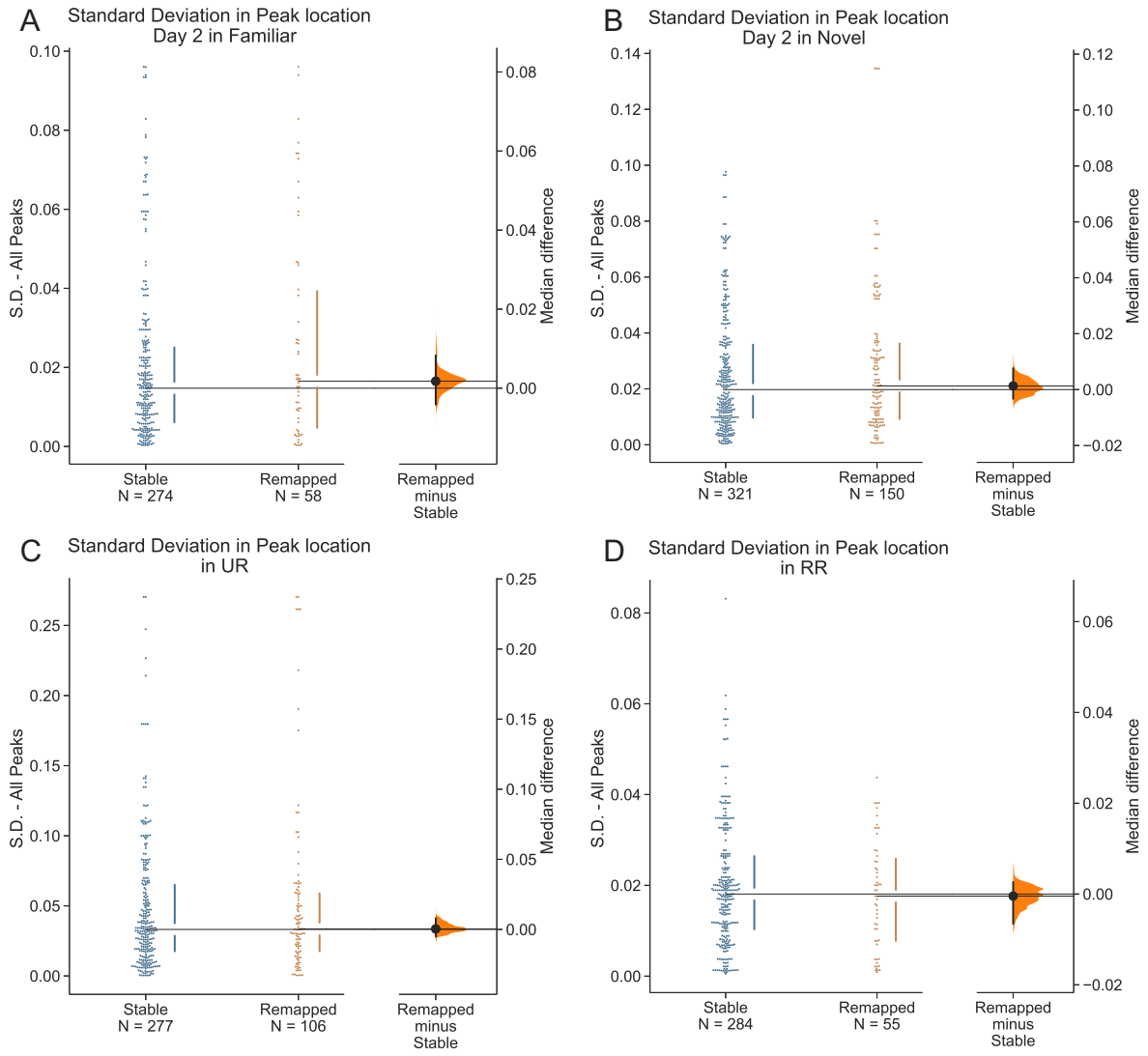

Figure 2.5: **Following the initial epoch, remapped and stable PFs have similar spatial precision during subsequent epochs**
(A) Comparison of spatial precision of PFs on day 2 in the familiar environment. Right, bootstrapped median difference between remapped vs stable PFs from day 1. 5000 re-samples, P = 0.421.
(B) Comparison of spatial precision of PFs on day 2 in the novel environment. Right, bootstrapped median difference between remapped vs stable PFs from day 1. 5000 re-samples, P = 0.811.
(C) Comparison of spatial precision of PFs in UR condition. Right, bootstrapped median difference between remapped vs stable PFs from R. 5000 re-samples, P = 0.869
(D) Comparison of spatial precision of PFs in RR condition. Right, bootstrapped median difference between remapped vs stable PFs from R. 5000 re-samples, P = 0.848

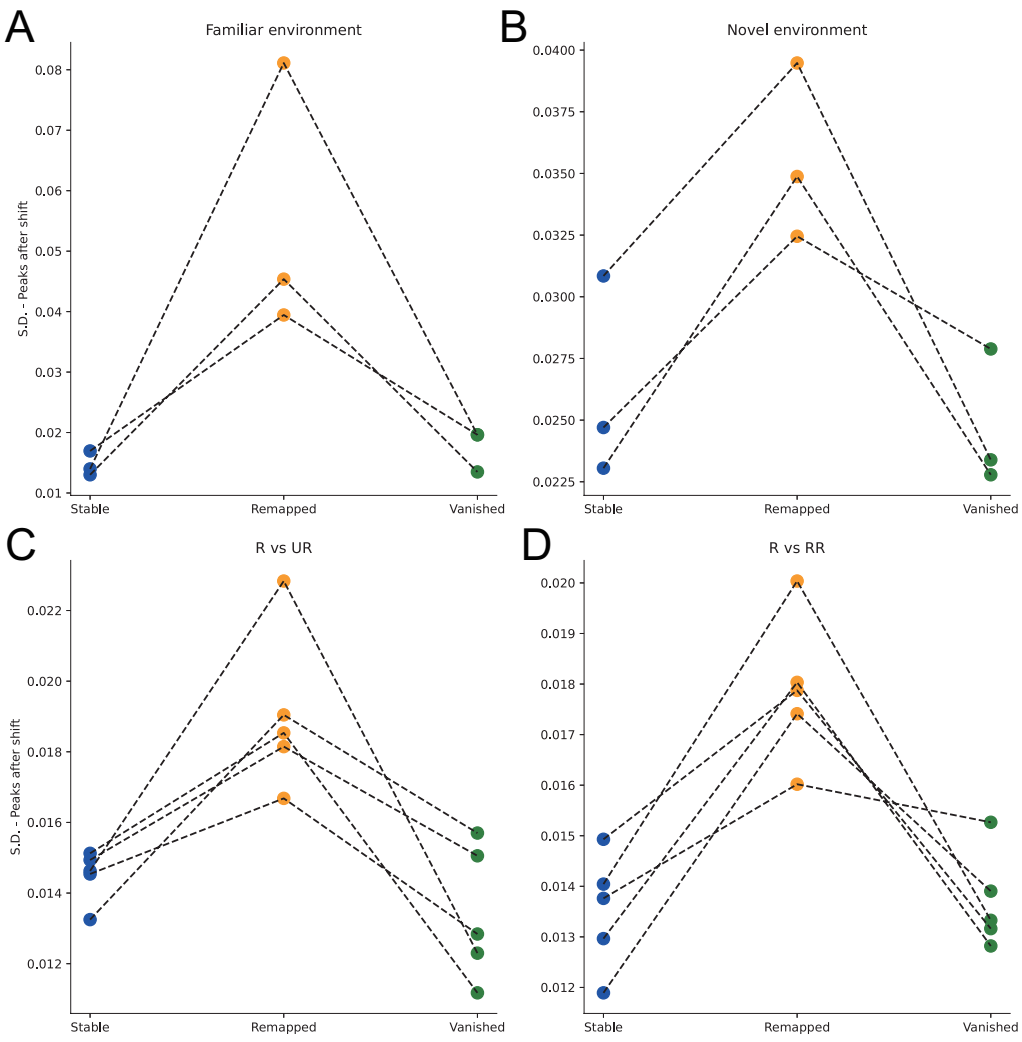

Figure 2.6: **Comparison of median spatial precision of place fields for individual animals.**

Figure 2.6 (continued): **Comparison of median spatial precision of place fields for individual animals**

(A) Median spatial precision (as measured by the standard deviation, S.D., of PF peaks) in each category for individual animals in the familiar environment. Significant differences between PF categories is shown using one-way ANOVA (F = 8.814, P = 0.0164), Tukey post-hoc test shows a significant difference for Stable vs Remapped (P = 0.0218), and for Remapped vs Vanished (P = 0.0300)

(B) Same as (A) but for novel environment. Significant differences between PF categories is shown using one-way ANOVA (F = 8.43, P = 0.01810), Tukey post-hoc test shows a significant difference for Stable vs Remapped (P = 0.0394), and for Remapped vs Vanished (P = 0.0212)

(C) Same as (A) but for the Rewarded (R)-Unrewarded (UR) experiment. PFs are categorized by their fate in UR but their spatial precision is measured in R. Significant differences between PF categories is shown using one-way ANOVA (F = 14.24, P = 0.000679), Tukey post-hoc test shows a significant difference for Stable vs Remapped (P = 4.15E-03), and for Remapped vs Vanished (P = 7.97E-04)

(D) Same as (A) but for the Rewarded (R)-re-rewarded (RR) experiment. PFs are categorized by their fate in RR following an epoch of UR, but their spatial precision is measured in R. Significant differences between PF categories is shown using one-way ANOVA (F = 21.05, P = 0.000119), Tukey post-hoc test shows a significant difference for Stable vs Remapped (P = 2.569E-04), and for Remapped vs Vanished (P = 3.71E-04).

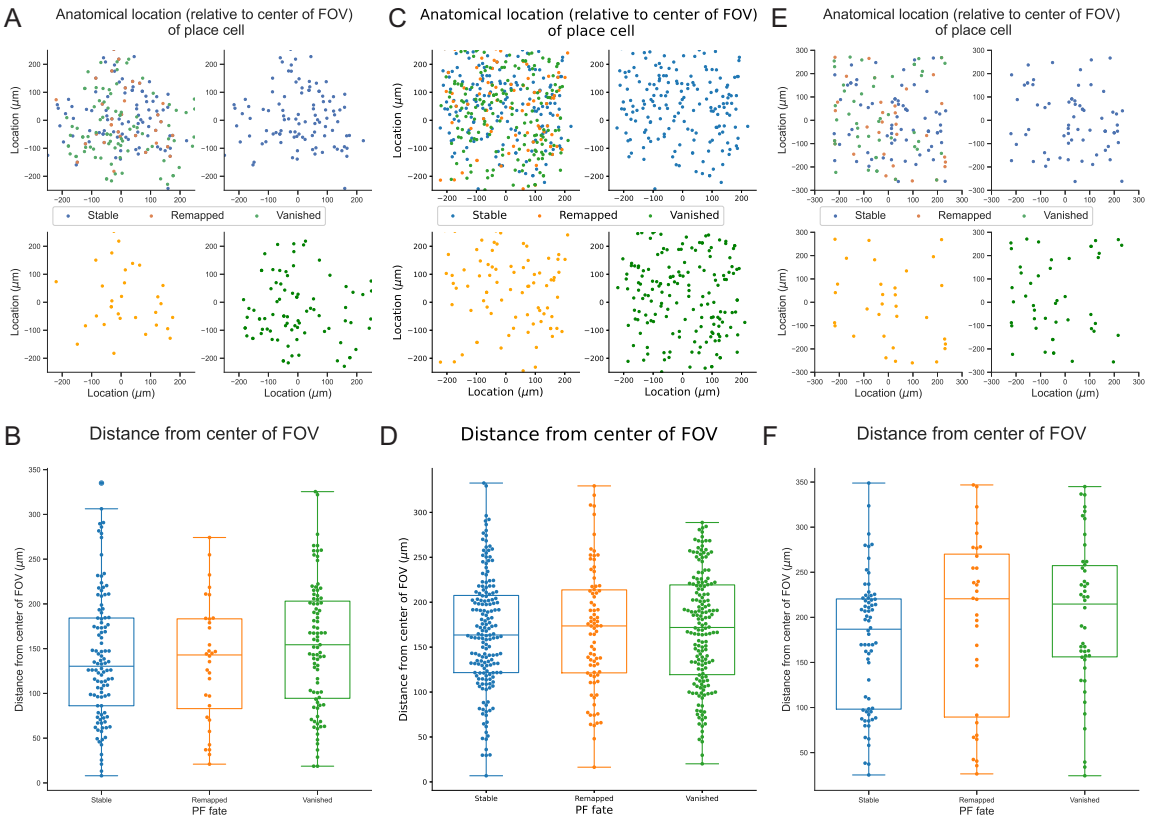

Figure 2.7: **Anatomical location of place cells color-coded based on their PF fate in three example animals**
(A) Anatomical location in x and y of place cells (relative to center of field of view (FOV)) in one example animal (#3, imaged across 2 days in familiar environment). Origin represents center of FOV.
(B) Comparison of anatomical location of place cells from center of FOV grouped by PF fate category (Stable, N = 108; Remapped, N = 32; Vanished, N = 87). One-way ANOVA shows no statistically significant difference between categories (F = 1.160, P = 0.315).
(C) Same as (A) but for a different animal (#4, imaged across 2 days in novel environment).
(D) Same as (B) but for animal #4 (Stable, N = 176; Remapped, N = 82; Vanished, N = 170). One-way ANOVA shows no statistically significant difference between categories (F = 0.157, P = 0.855).
(E) Same as (A) but for a different animal (imaged across blocks of trials with changing reward (R-UR-RR)). PFs from R are categorized by their fate in UR.
(F) Same as (B) but for the animal in (E) (Stable, N = 68; Remapped, N = 32; Vanished, N = 46). One-way ANOVA shows no statistically significant difference between categories (F = 1.896, P = 0.154).

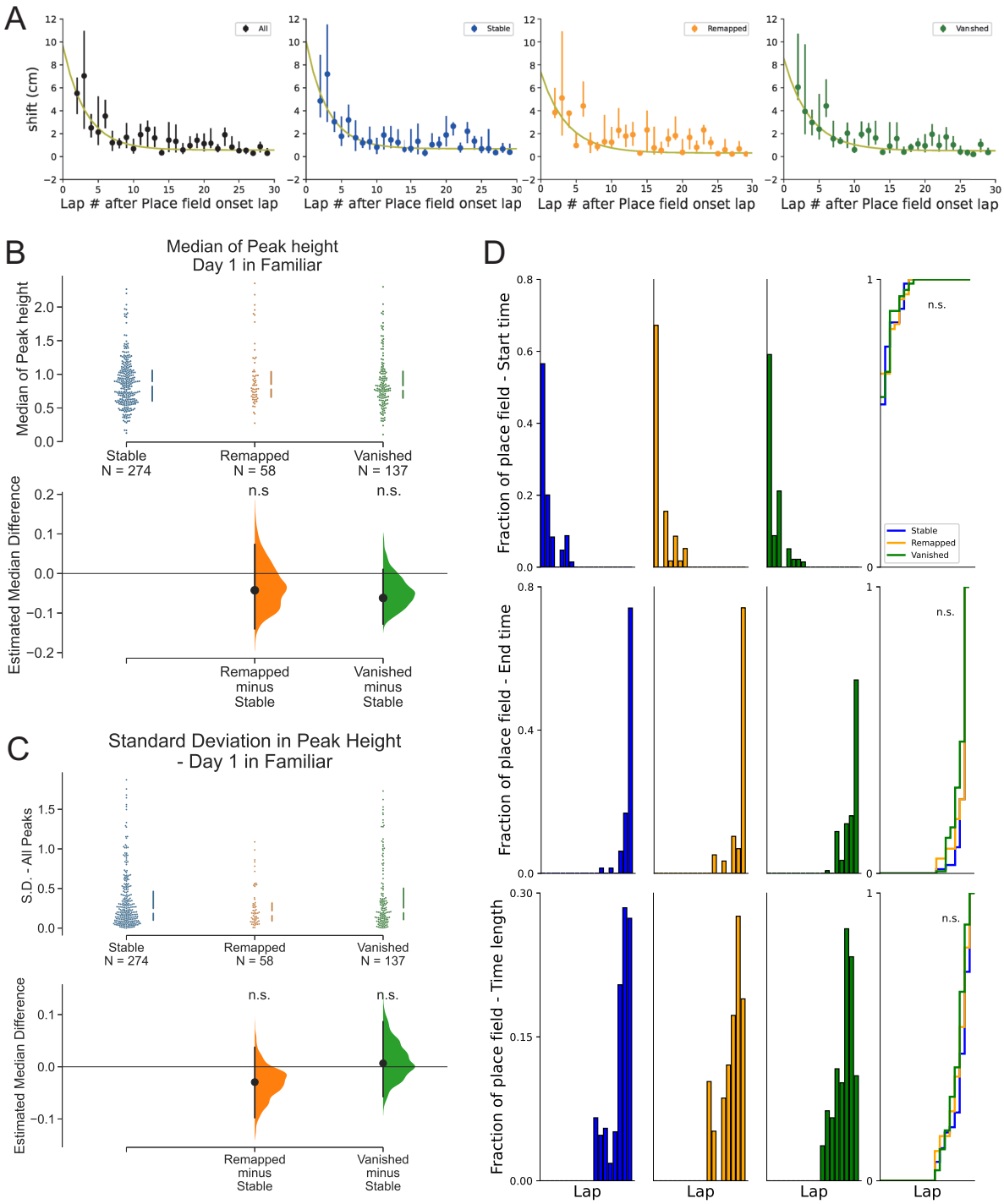

Figure 2.8: **Other place field metrics are not associated with place field fate across days in a familiar environment.**

Figure 2.8 (continued): **Other place field metrics are not associated with place field fate across days in a familiar environment**
(A) Comparison of backward shifting dynamics between the different PF fate categories. Fitting parameters for the exponential $F(x) = Ae^{-x/T}$: For shift of all PFs: $A = 9.1 \pm 4.3$, $T = 3.2 \pm 1.1$; For stable PFs: $A = 9.4 \pm 6.7$, $T = 3.0 \pm 1.4$; For remapped PFs: $A = 7.1 \pm 3.9$, $T = 3.6 \pm 1.3$; For vanished PFs: $A = 8.0 \pm 5.3$, $T = 3.7 \pm 1.5$;
(B) Comparison of median of peak amplitude. P = 0.577 for stable vs remapped, 5000 re-samples, P = 0.210 for stable vs vanished
(C) Comparison of lap-by-lap peak amplitude variation. P = 0.313 for stable vs remapped, 5000 re-samples, P = 0.915 for stable vs vanished.
(D) Histograms of PF onset laps, end laps, and duration (in laps) for Stable, Remapped and Vanished PFs. Cumulative fraction plots (right). Wilcoxon rank-sum test, for stable vs remapped: start time: P = 0.160, end time: P = 0.815, time length: P = 0.918; for stable vs vanished: start time: P = 0.884, end time: P = 0.907, time length: P = 0.941; for remapped vs vanished: start time: P = 0.173, end time: P = 0.953, time length: P = 0.965

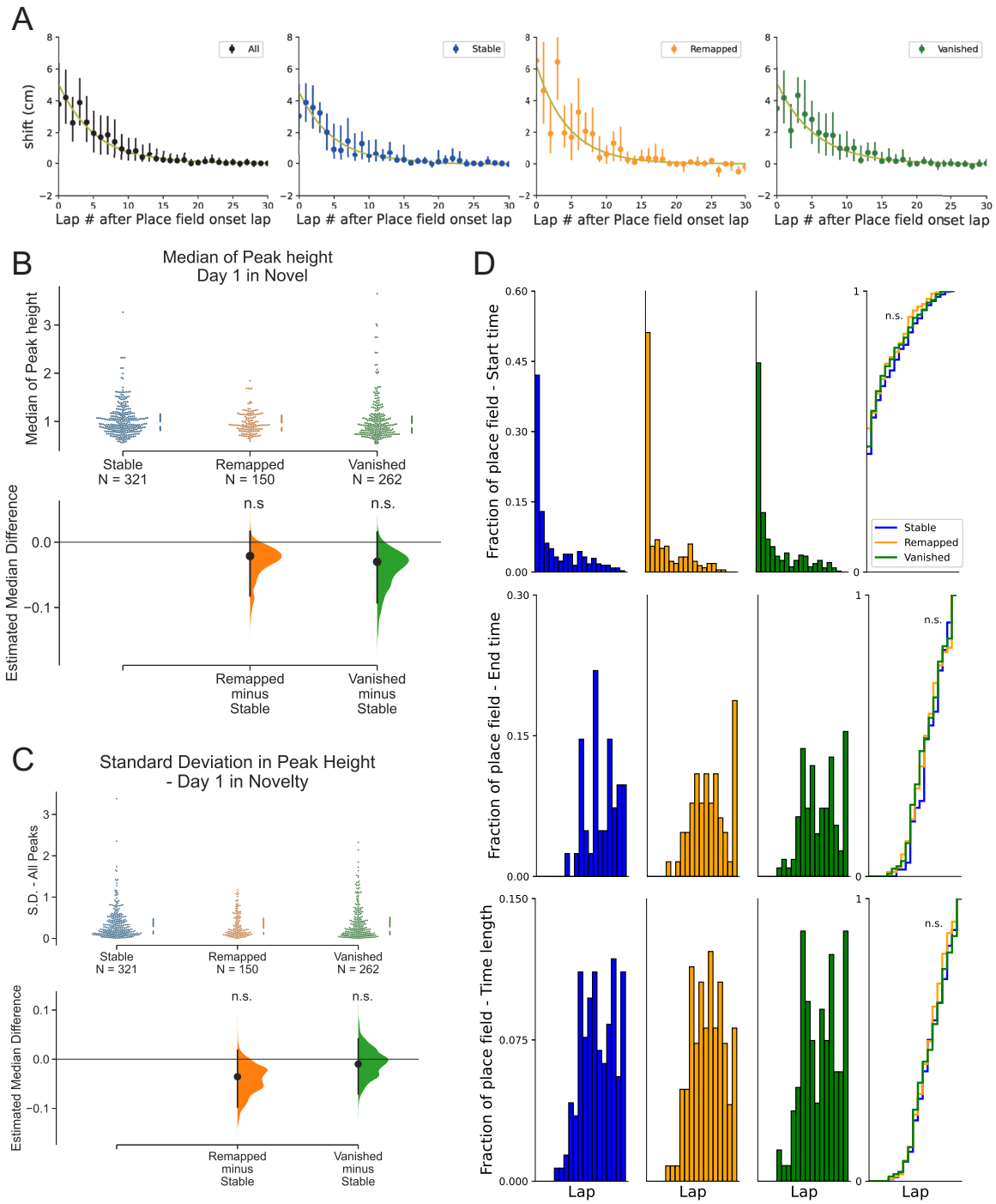

Figure 2.9: **Other place field metrics are not associated with place field fate across days in a novel environment**

Figure 2.9 (continued): **Other place field metrics are not associated with place field fate across days in a novel environment**
(A) Comparison of backward shifting dynamics between the different categories of PF fate. Fitting parameters for the exponential $F(x) = Ae^{-x/T}$: For shift of all PFs: $A = 5.0 \pm 1.3$, $T = 5.3 \pm 1.0$; For stable PFs: $A = 4.6 \pm 1.0$, $T = 5.0 \pm 0.9$; For remapped PFs: $A = 6.2 \pm 1.8$, $T = 4.5 \pm 0.9$; For vanished PFs: $A = 5.1 \pm 1.3$, $T = 5.4 \pm 1.0$;
(B) Comparison of median of peak amplitude. P = 0.259 for stable vs remapped, 5000 resamples, P = 0.094 for stable vs vanished.
(C) Comparison of lap-by-lap peak amplitude variation. P = 0.223 for stable vs remapped, 5000 resamples, P = 0.847 for stable vs vanished.
(D) Histograms of PF onset laps, end laps, and duration (in laps) for stable, remapped and vanished PFs. Cumulative fraction plots (right). Wilcoxon rank-sum test, for stable vs remapped: start time: P = 0.474, end time: P = 0.704, time length: P = 0.883; for stable vs vanished: start time: P = 0.589, end time: P = 0.616, time length: P = 0.930; for remapped vs vanished: start time: P = 0.759, end time: P = 0.953, time length: P = 0.998

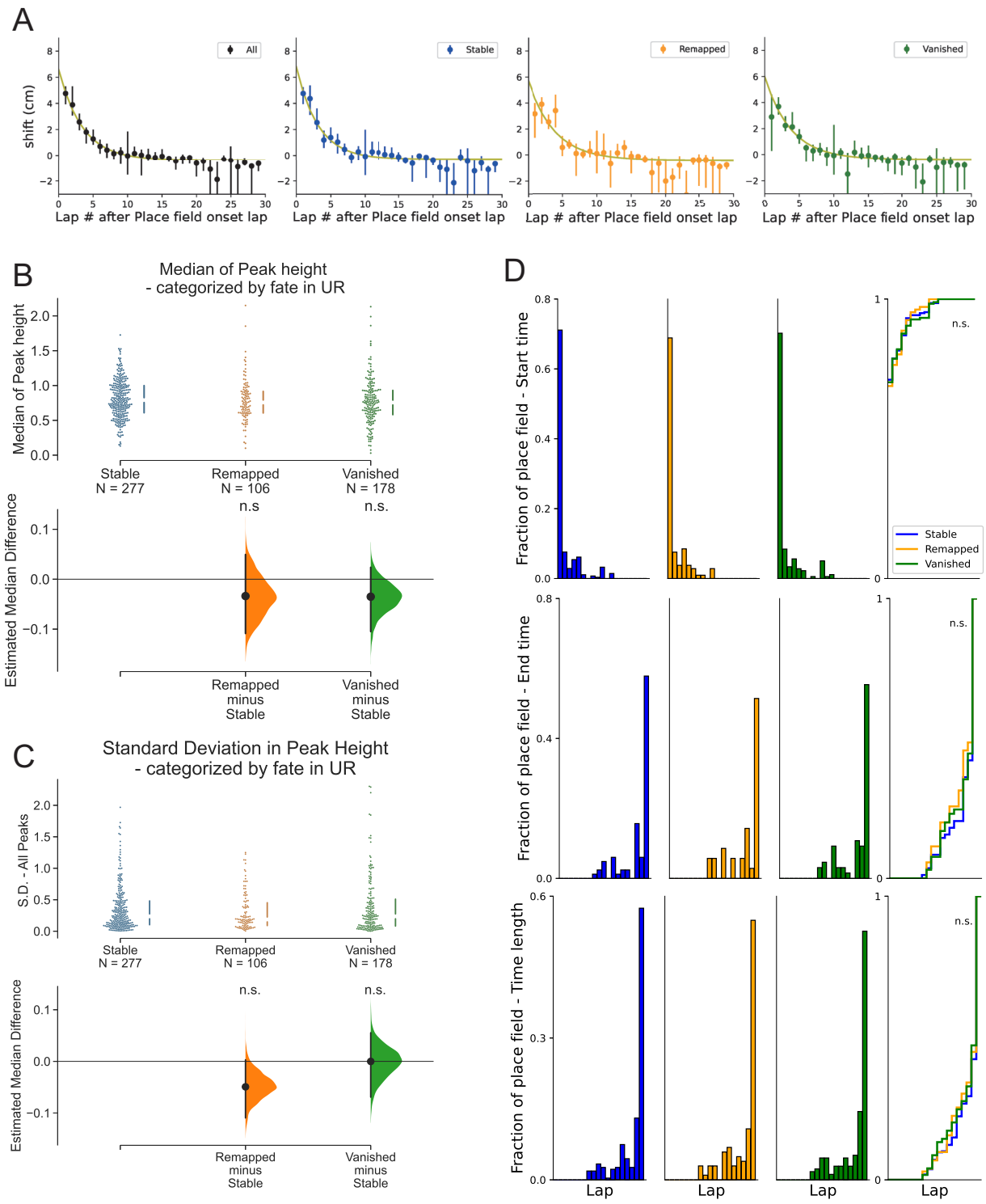

Figure 2.10: **Other place field metrics in R are not associated with place field fate in UR**

Figure 2.10 (continued): **Other place field metrics in R are not associated with place field fate in UR**
(A) Comparison of backward shifting dynamics between the different categories of PF fate. Fitting parameters for the exponential $F(x) = Ae^{-x/T}$: For shift of all PFs: $A = 7.0 \pm 1.2$, $T = 3.4 \pm 0.7$; For stable PFs: $A = 7.1 \pm 1.3$, $T = 3.2 \pm 0.7$; For remapped PFs: $A = 6.1 \pm 1.7$, $T = 3.8 \pm 1.1$; For vanished PFs: $A = 6.4 \pm 1.6$, $T = 3.8 \pm 1.1$;
(B) Comparison of median of peak amplitude. P = 0.437 for stable vs remapped, 5000 re-samples, P = 0.2472 for stable vs vanished.
(C) Comparison of lap-by-lap peak amplitude variation. P = 0.140 for stable vs remapped, 5000 re-samples, P = 0.996 for stable vs vanished.
(D) Histograms of PF onset laps, end laps, and duration (in laps) for stable, remapped and vanished PFs. Cumulative fraction plots (right). Wilcoxon rank-sum test, for stable vs remapped: start time: P = 0.475, end time: P = 0.792, time length: P = 0.850; for stable vs vanished: start time: P = 0.759, end time: P = 0.977, time length: P = 0.804; for remapped vs vanished: start time: P = 0.511, end time: P = 0.770, time length: P = 0.965

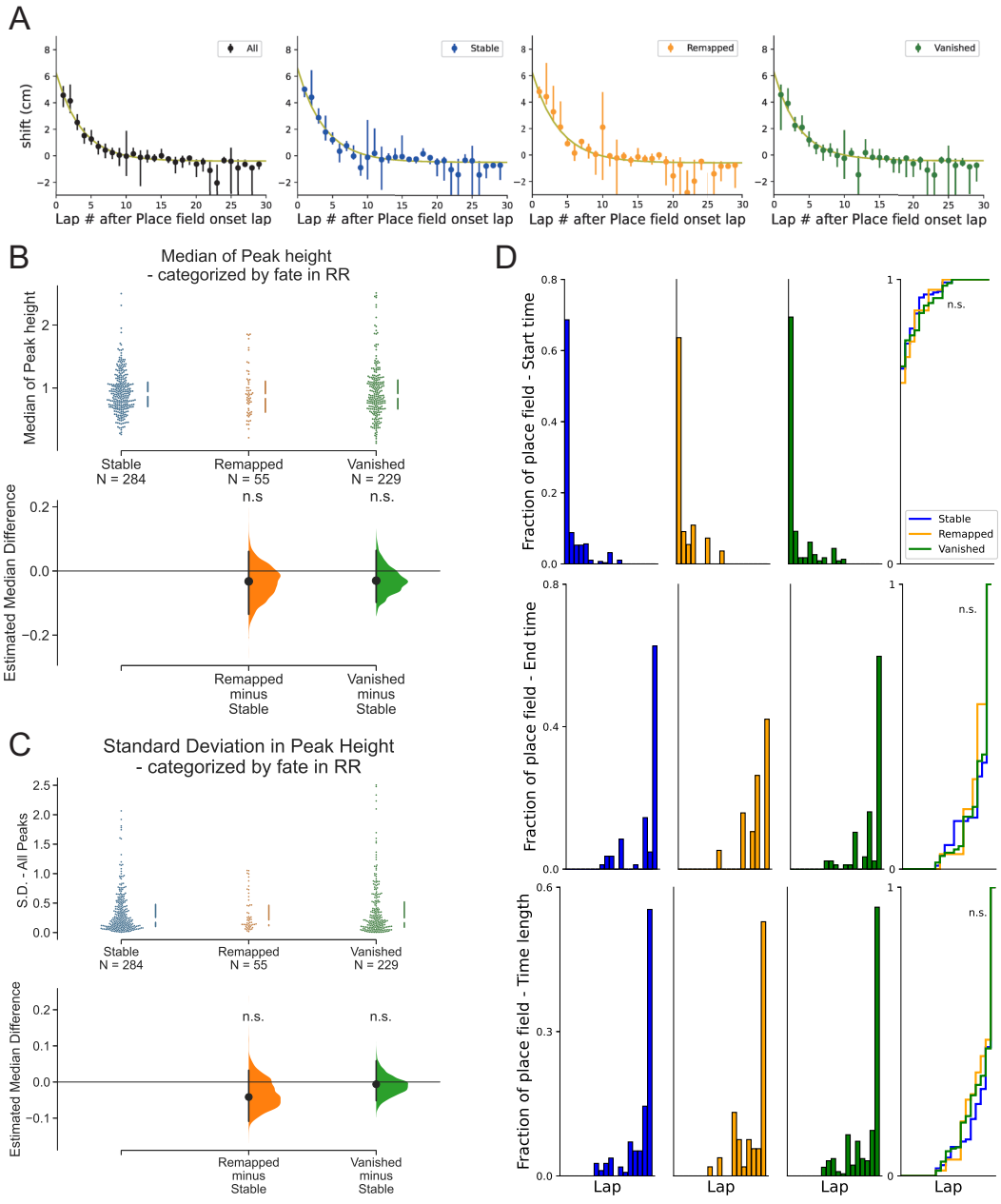

Figure 2.11: **Other place field metrics in R are not associated with place field fate in RR**

Figure 2.11 (continued): **Other place field metrics in R are not associated with place field fate in RR**
(A) Comparison of backward shifting dynamics between the different categories of PF fate. Fitting parameters for the exponential $F(x) = Ae^{-x/T}$: For shift of all PFs: $A = 6.6 \pm 1.2$, $T = 3.6 \pm 0.8$; For stable PFs: $A = 7.1 \pm 0.9$, $T = 3.8 \pm 0.7$; For remapped PFs: $A = 6.8 \pm 0.8$, $T = 3.9 \pm 0.7$; For vanished PFs: $A = 6.7 \pm 2.0$, $T = 3.5 \pm 1.0$;
(B) Comparison of median of peak amplitude. P = 0.567 for stable vs remapped, 5000 re-samples, P = 0.466 for stable vs vanished.
(C) Comparison of lap-by-lap peak amplitude variation. P = 0.338 for stable vs remapped, 5000 re-samples, P = 0.680 for stable vs vanished.
(D) Histograms of PF onset laps, end laps, and duration (in laps) for stable, remapped and vanished PFs. Cumulative fraction plots (right). Wilcoxon rank-sum test, for stable vs remapped: start time: P = 0.737, end time: P = 0.884, time length: P = 0.965; for stable vs vanished: start time: P = 0.650, end time: P =0.965, time length: P = 0.895; for remapped vs vanished: start time: P = 0.965, end time: P = 0.838, time length: P = 0.988

CHAPTER 3

HIPPOCAMPAL REPLAY MODULATED BY EXPERIENCE

3.1 Introduction

As discussed in 1, replay is an important mechanism supporting memory processing in the hippocampus. This serves as a great proxy to investigate the formation, consolidation and retrieval of memory. We discussed the association between PF preciseness and representational drift in Chapter 2. We suggested that synaptic plasticity is the driving mechanism of drift. Replay, a reactivation of place cell sequences, can well induce synaptic plasticity (Sadowski et al., 2016) and hence stabilize, or update the place cell assembles.

Forward and reverse replay are shown to play different roles in memory (Shin et al., 2019). Reverse replays rate are modulated by reward, while forward replays are not (Ambrose et al., 2016). In Bhattarai et al. (2020), results showed while the the reverse replay rate was enhanced by reward, for forward replay, the fidelity was enhanced instead. Because we investigated the representational drift across reward changing episodes, we also wanted to know how forward and reverse replay events were influenced by this scenario.

In this work, we wanted to replicate the result of reward's effect on replay using 2-photon calcium imaging, which can record a large ensemble of neurons at the same time. We next investigated how the flip-side of reward - fear - effects replay events by using contextual fear conditioning. This work provides insight into how positive and negative experiences influence the dynamics of replay events in CA1.

3.2 Materials and Method

Methods to extract place cell and PFs are descirbed previously (See 2.2).

3.2.1 Sub-frame time precision of place cell activity

As replays are of short time scales (200ms), we needed a measure of sub-frame precision of the time of the transient. To achieve this, first, reference transients for each cell were obtained, by calculating the median across all transients of that cell in the particular imaging session. An example of the reference transient is shown in Fig. 3.1A. The cross correlation between each transient and the reference were then obtained, and fitted to a Gaussian function. The peak of the Gaussian fit were then used as the 'precise time' of the transient.

3.2.2 Replay sequence

The at-rest activity of the cells were collected and events of synchronous firing were identified if more than 5 cells are active in a time window of 6 frames (200 ms). The 'precise' time of each transients involved in the synchronous event were then obtained and sorted. The event would be considered a 'replay' if the Spearman correlation between the time and PF location of the cell has a P-value <0.05. Fig. 3.1C showed the PF sequence of a sample session, and Fig. 3.1D showed an example replay event. The cells involved in the replay were marked in Fig 3.1C with corresponding color.

3.2.3 Fidelity of the replay

To obtain the fidelity of the replay, we first applied a Bayesian decoding algorithm to estimate the animal's location. Activities of neurons imaged were collected with the behavioural data. When the animal is in motion, for each transient, the location of the animal was recorded. Then the probability of the animal being in a location bin, given activity of a particular cell,

would be given by $P(x) = N(x)/N_{tot}$, where $N(x)$ is the number of times that the animal is found in the particular location when the cell fires. With the probability for all cells, we then construct the conditional probability for animal location, when given the activity of the cells. Fig. 3.1E shows the performance of the decoder on a particular lap in a particular session and the same decoder was used to decode a replay event. Fig. 3.1F showed a replay with the decoded location. The fidelity was then defined by the Spearman correlation between the decoded location and the 'precise' time. Only events with P-value$<$0.01 are counted as replay.

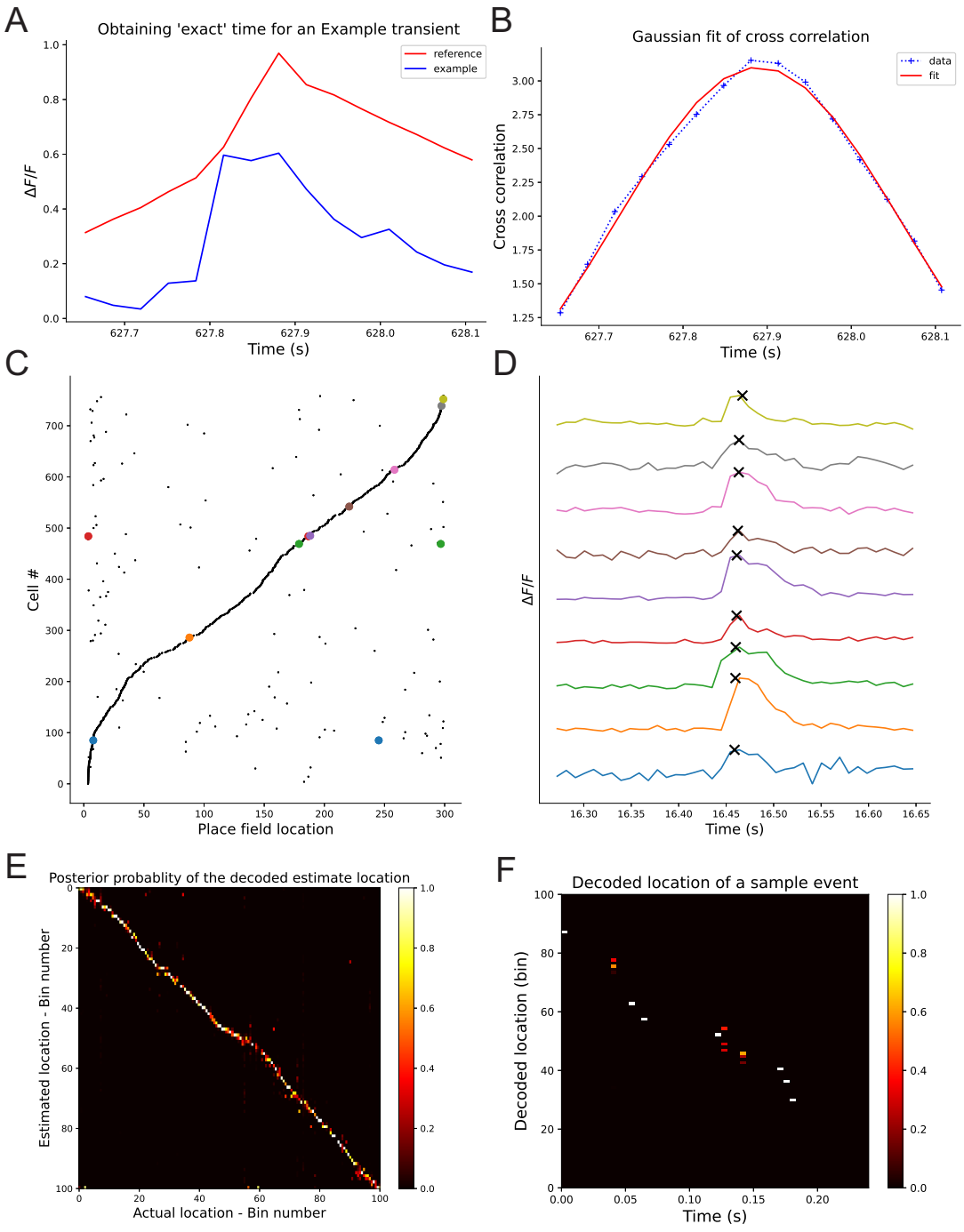

Figure 3.1: **Illustration of method applied to study replay**.

Figure 3.1 (continued): **Illustration of method applied to study replay**
(A) Example transient and the reference transient of a sample cell
(B) Cross-correlation of the example transient with the reference, and its Gaussian fit, returning $t_{peak} = 6.27890E + 02$
(C) PF sequence of an example session, sorted with their PF locations. Color dots correspond to the cells involved in the example replay in (D)
(D) An example replay with the Calcium transient of the cells. The crosses indicate the 'precise' time of the transient.
(E) Decoded location vs actual location for an example lap
(F) Decoded location vs time of a sample replay event (different from (D)). For plotting, time is binned into 100 bins. Pearson correlation: R=-0.9283, P=0.0001

3.3 Result

3.3.1 Hippocampal replay modulated by reward contingencies

We analyzed replay events for the experiment with changes in reward contingencies (Krishnan et al., 2022). The experimental design is described in Fig. 2.3A. The rate of replay of the PF sequence in R when animals were at rest in each episode (R, UR and RR) were obtained 3.2. Interestingly, we found that the replay rate in UR was much lower than that in R and RR. This indicates that the replay rate of place cell sequences is modulated by the change in reward expectation even when animals are in the same spatial environment. Because replay events have been associated with memory consolidation, this suggests that when rewards are not expected during an experience, that experience is less likely to be consolidated through a drop in replay rate. The connection between reward and replay has been previously established using electrophysiological techniques (Foster and Wilson, 2006; Singer and Frank, 2009; Ambrose et al., 2016; Bhattarai et al., 2020). However, our results were generated using 2-photon calcium imaging, suggesting that replay events can be reliably detected in calcium imaging data-sets.

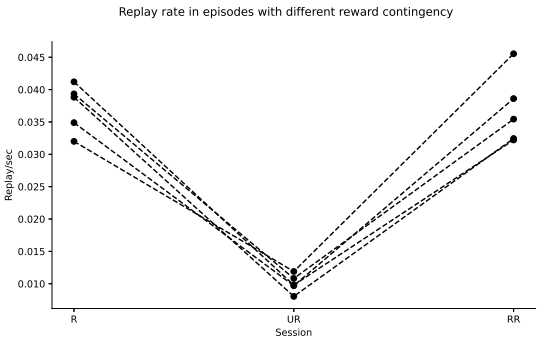

Figure 3.2: **Replay rate in blocks of trials with different reward contingencies** Replay rate were compared for R, UR and RR, n=5.

3.3.2 Hippocampal replay modulated by fear experience

We then analyzed replay events throughout contextual fear conditioning. The experimental design is described in Fig. 3.3A. The animal showed behavioural learning by displaying increased freezing when re-introduced to the shocked environment (CFC) on day 3. The replay rate during rest periods in each episode were again obtained. Because animals were exposed to two different environments, we assessed replay rates of the place cell sequences associated with each environment independently and separated forward and reverse replay events. We found that the replay rate of the familiar environment (unshocked environment) remained roughly constant during rest (Fig. 3.3B) in both environments across all days which consisted of a preshock day (day 1), a shock day (day 2) and two postshock days (days 3 and 4). However, the total replay rate (meaning both forward and reverse replay added together) of the CFC environment (shocked environment on day 2) increased drastically on day 3 in the CFC environment (Fig. 3.3C), which was one day following shocks in that environment. This indicates that the replay rate of an environment increases following a learned association with fear, suggesting a role in fear memory retrieval.

We next analyzed the fidelity of the replay events. The fidelity of the forward replays was roughly constant, across all sessions and all days, both pre-shock and post-shock. But re-

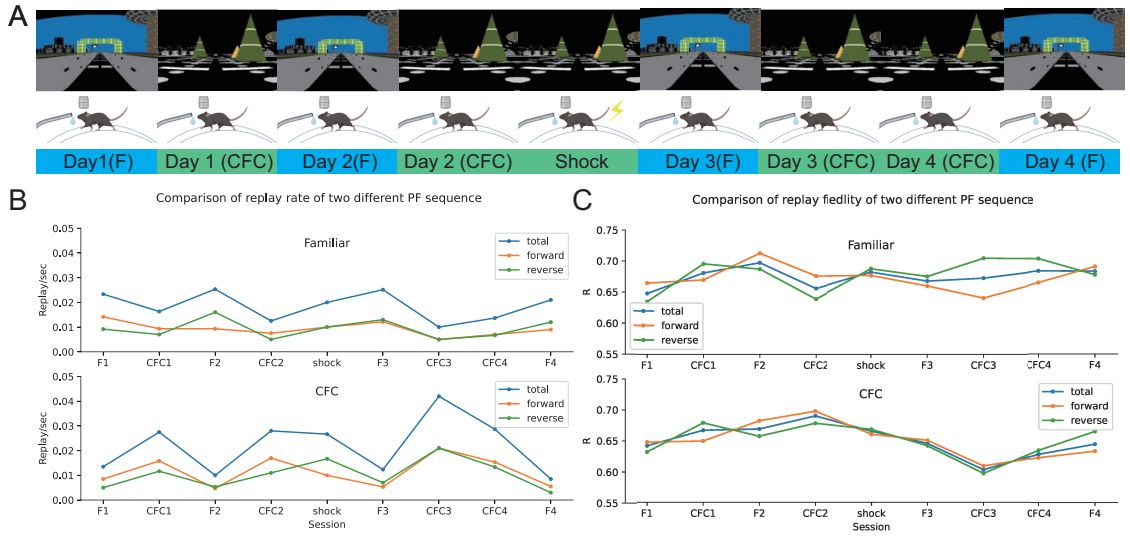

Figure 3.3: **Replay in contextual fear conditioning**
(A) Experiment protocol. Top: the familiar environment (F) and the environment with shock experience (CFC). Bottom: The animal was shocked on day2 and imaged day 1-4
(B) Replay rate (total, forward and reverse) in each session
(C) Replay fidelity (total, forward and reverse) in each session

verse replay fidelity dropped significantly when the animal was re-introduced to the shocked environment on day 3. While this may hint that the fidelity of replay events changes following CFC, the more plausible explanation of this result is that there is partial remapping of the spatial map after CFC. Because we are comparing replay events to the before-shock place cell sequence, fidelity might decrease if replay events contain sequences closer to the new place cells sequences that develop following CFC. More analysis is needed to determine what is driving the decrease in replay fidelity post-CFC before any conclusions can be made. Regardless of the cause, forming a fear association with an environment changes spatial activity dynamics in CA1, either through remapping of PFs during navigation and/or through changes in replay fidelity.

3.4 Discussion

As stated in Introduction, the replay rate has been shown to be modulated by reward expectation (Foster and Wilson, 2006; Singer and Frank, 2009; Ambrose et al., 2016; Bhattarai et al., 2020). Our results agree with the literature. When the animal behaviorally learned to stop licking under the new reward expectation (UR), the replay rate changed by dropping significantly. This indicates that replay rate is associated with reward and may serve to consolidate salient events into long-term memory. Importantly, we replicated this finding from data obtained using 2-photon calcium imaging. Compared with electrophysiology, the primary method for studying replay as it provides single spike resolution, calcium imaging is slow. There are multiple components in the process that determine temporal resolution, such as the dynamics of calcium influx, the dynamics of calcium binding and unbinding to GCaMP, and the scanning speed of the microscope. Furthermore, current GCaMPs are unable to resolve single spikes in vivo. Together, this means the temporal resolution with 2-photon calcium imaging is on the scale of a 10s to 100s of ms and is unable to detect single spikes. Replay sequences occur on rapid timescales on the range of 10s ms, and each cell only fires 1 to 5 spikes. This pushes up against the limits of 2-photon calcium imaging. However, our method of detecting calcium transient peaks gives us sub-frame resolution, and given our replicated finding of replay rates associated with rewards, we are confident we are able to detect replay events using 2-photon calcium imaging. We may be missing single spikes and may not be able to pull out every replay event that is occurring, but the high number of cells that can be co-recorded with 2-photon calcium imaging likely more than offsets this issue. further, because 2-photon imaging allows for longitudinal tracking of the same cells across many days, it opens up a new area of investigation regarding how replay events change across long timescales, something not possible with electrophysiology.

For the fear conditioning experiment, we observed that replay rate drastically increased when the animal was reintroduced to the environment that they had associated with fear. The fear memory was apparent in the animals behavior, as they froze more often and for a longer time. Therefore, contextual fear learning is associated with the enhancement of replay rate. One can argue that the enhancement of replay rate is a neural correlate of fear memory retrieval that then drives the innate fearful freezing behavior. To test this, one possible idea would be to check whether those replays events are more associated to their future trajectory/position from their current position during freezing. If yes, it would suggest that the replays are associated to the animal recalling their past fear experience in the environment.

Replay fidelity also showed a significant change following CFC. However, this could be explained by the partial remapping of the spatial encoding. The animal learned the fear association and this could be reflected through changes in the hippocampal spatial code represented by changes in PFs of place cells. Comparing the PFs sequence before shock with replay happening in sessions with remapped PF sequences after shock could naturally show a lower replay fidelity. To study the effect of the fear memory on replay fidelity, one has to remove the effect of remapping. We have not done this analysis, so do not know if replay fidelity is disrupted following CFC or if spatial remapping has occurred. Teasing these apart should be the focus of future replay investigations as they might provide deep insight into hippocampal memory processing and the role of replay.

CHAPTER 4

CONCLUSION AND FUTURE DIRECTIONS

4.1 Summary of Findings

In The Precision of Place Fields Governs Their Fate Across Epochs of Experience, we showed that the preciseness of PFs during navigation is related to their fate, or drift, across episodes of experience. This association is true for drift across distinct chunks of time and across changes in rewards expectation, both of which can be thought of as distinct episodes. We proposed a model that connects the precision of PFs during navigation to representation drift that involves synaptic plasticity at CA1-CA3 synapses occurring on short timescales (during navigation) that leads to longer-lasting changes that manifest on timescales associated with drift.

Similarly, we investigated place cell sequence replay (rate and fidelity) throughout a reward-changing paradigm and throughout contextual-fear-conditioning across multiple days. Both involved learning of novel information occurring in the same spatial environment. For the reward-changing paradigm, the replay rate significantly dropped during trials that were unrewarded, and the rate restored when the animal was re-rewarded. For the contextual fear conditioning experiment, the total replay rate of the familiar environment remained at the same level for both shocked (F) and unshocked (CFC) environment, both pre-shock and post-shocked. However, the replay rate for the shocked environment showed a significant increase when the animal was re-introduced to the shocked environment (CFC) post-shock.

4.2 Discussion and Future directions

First, the study can be extended to CA3. CA3 is the main excitatory upstream input to CA1. It is known that CA3 PFs are more stable (less drift) (Dong et al., 2021). We can

check if CA3 demonstrates the same association between PF preciseness and drift. It may be the case that PFs are more precise across the population, which would explain the lack of drift and would suggest the same synaptic mechanisms are at play in CA3 and CA1. If PF precision and drift and not associated in CA3, it would suggest major differences in synaptic plasticity at CA3-CA1 synapses compared to DG-CA3 synapses (DG is the main excitatory input to CA3). Any differences may also give insights into distinct roles of CA1 and CA3 in memory processing. The auto-associative structure of CA3 circuit is well adapted for rapid storage and retrieval of memories. Mice were shown to exhibit deficits in one-trial memory tasks under impairment in plasticity of CA3-CA3 or DG-CA3 connections (Rebola et al., 2017). This auto-associative structure also allows associations between spatial location, objects or reward, and enables completion of patterns from fragments of information to drive complete recall. Some data has shown support for the pattern completion function of CA3 (Knierim and Neunuebel, 2016). Modeling also supports how the CA3 network with sparse connectivity generates pattern completion (Guzman et al., 2016). The recurrent connection in CA3 can also result in different plasticity rules than in CA1. In fact, the effect of spatial novelty on plasticity has been shown to be different for CA1 and CA3 (Roth et al., 2012b).

To further investigate representation drift in both regions and its relationship to PF precision as well as how these regions interact, a possible experiment would be to image both regions at the same time and identify co-activated ensembles in the regions. We can then investigate PF preciseness and drift under the same conditions, and also co-activation rates across regions. As reported in Nakazawa et al. (2002), CA3 N-methyl-D-asparate (NMDA) receptors are required for associative memory recall. We could then use NMDAR blockers to observe its effects on drift, PF precision, and co-active ensembles in CA1 and CA3 to further connect these processes to memory function.

To help develop further synaptic level insights we could build a computational model of the CA1 network. This could help test the feasibility of our conceptual model by revealing whether biologically plausible plasticity rules are engaged over the timescale and repeated trials similar to our experiments to produce the representation drift we observed. It is supported by Bittner et al. (2017) that a newly discovered plasticity rule in CA1 is important for PF formation and is a non-Hebbian rule. This has been given the name behavioural time scale synatic plasticity (BTSP) as it acts over a timescale of seconds, rather than the more classic hebbian rule of spike-timing dependent plasticity (STDP) which acts over milliseconds. We can apply such a plasticity rule in a computational model to check if it can influence both preciseness of PFs and drift.

We found that the day 2 lap-by-lap dynamics show no relationship with their prior PF defined on the previous day. This means that PFs can switch categories. For instance, we claim that remapped PF can become stable PF and vice versa. In order to prove this, experiments need to be extended to longer time periods that go beyond two consecutive days. This would help us understand the day-by-day dynamics along with their lap-by-lap dynamics within sessions on each day. This would provide further insight into the processes of remapping. We could determine whether there are specific ensembles of cells that spatially remap to encode new episodes/sessions, or whether all place cells could potentially remap. For instance, If previously remapped PFs can then become stable PFs (or vice versa), that would indicate that the cell ensemble is flexible and synaptic plasticity is the likely driver of remapping dynamics. If cells stay within specific categories, e.g., stable cells are always stable, this would indicate cells are preconfigured to to express specific dynamics and the network is somewhat hardwired.

As shown in Fig 1.1, the dentate gyrus (DG) is the first stage of hippocampus. In Knierim and Neunuebel (2016), data supports theories of pattern separation in DG, a key process in which similar memories can be separated within the network. In order to fully understand how spatial memories are formed and updated, we must therefore extend our investigation to understanding the dynamics in DG and how they influence processes in CA1 and CA3. More specifically, we can study drifts/change in DG representations and also trial-by-trial preciseness of such representations, as we did in CA1. This should help reveal how much drift is inherited from upstream processing in DG. Together, these studies should reveal how different regions in hippocampus connect together to support memory formation/consolidation/retrieval.

REFERENCES

Ambrose RE, Pfeiffer BE, Foster DJ. Reverse Replay of Hippocampal Place Cells Is Uniquely Modulated by Changing Reward. Neuron. 2016 Sep; 91(5):1124–1136. https://doi.org/10.1016/j.neuron.2016.07.047, doi: 10.1016/j.neuron.2016.07.047.

Andersen P, Morris R, Amaral D, Bliss T, O'Keefe J. The Hippocampus Book. Oxford University Press; 2006. https://doi.org/10.1093/acprof:oso/9780195100273.001.0001, doi: 10.1093/acprof:oso/9780195100273.001.0001.

Barry C, Burgess N. Learning in a geometric model of place cell firing. Hippocampus. 2007; 17(9):786–800. https://onlinelibrary.wiley.com/doi/abs/10.1002/hipo.20324, doi: https://doi.org/10.1002/hipo.20324.

Berners-Lee A, Feng T, Silva D, Wu X, Ambrose ER, Pfeiffer BE, Foster DJ. Hippocampal replays appear after a single experience and incorporate greater detail with more experience. Neuron. 2022; 110(11):1829–1842.e5. https://www.sciencedirect.com/science/article/pii/S089662732200246X, doi: https://doi.org/10.1016/j.neuron.2022.03.010.

Bhattarai B, Lee JW, Jung MW. Distinct effects of reward and navigation history on hippocampal forward and reverse replays. Proceedings of the National Academy of Sciences. 2020; 117(1):689–697. https://www.pnas.org/doi/abs/10.1073/pnas.1912533117, doi: 10.1073/pnas.1912533117.

Bittner KC, Milstein AD, Grienberger C, Romani S, Magee JC. Behavioral time scale synaptic plasticity underlies CA1 place fields. Science. 2017; 357(6355):1033–1036. https://www.science.org/doi/abs/10.1126/science.aan3846, doi: 10.1126/science.aan3846.

Broadbent NJ, Squire LR, Clark RE. Reversible hippocampal lesions disrupt water

maze performance during both recent and remote memory tests. Learn Mem. 2006 Mar; 13(2):187–191.

Carr MF, Jadhav SP, Frank LM. Hippocampal replay in the awake state: a potential substrate for memory consolidation and retrieval. Nature Neuroscience. 2011 Feb; 14(2):147–153. https://doi.org/10.1038/nn.2732, doi: 10.1038/nn.2732.

Colgin LL, Moser EI, Moser MB. Understanding memory through hippocampal remapping. Trends in Neurosciences. 2008; 31(9):469–477. https://www.sciencedirect.com/science/article/pii/S0166223608001677, doi: https://doi.org/10.1016/j.tins.2008.06.008.

Davoudi H, Foster DJ. Acute silencing of hippocampal CA3 reveals a dominant role in place field responses. Nature Neuroscience. 2019 Mar; 22(3):337–342. https://doi.org/10.1038/s41593-018-0321-z, doi: 10.1038/s41593-018-0321-z.

Deitch D, Rubin A, Ziv Y. Representational drift in the mouse visual cortex. Current Biology. 2021; 31(19):4327–4339.e6. https://www.sciencedirect.com/science/article/pii/S0960982221010526, doi: https://doi.org/10.1016/j.cub.2021.07.062.

Devalle F, Roxin A. Network mechanisms underlying representational drift in area CA1 of hippocampus. bioRxiv. 2022; https://www.biorxiv.org/content/early/2022/12/27/2022.11.10.515946, doi: 10.1101/2022.11.10.515946.

Diba K, Buzsáki G. Forward and reverse hippocampal place-cell sequences during ripples. Nature Neuroscience. 2007 Oct; 10(10):1241–1242. https://doi.org/10.1038/nn1961, doi: 10.1038/nn1961.

Dombeck DA, Harvey CD, Tian L, Looger LL, Tank DW. Functional imaging of hippocampal place cells at cellular resolution during virtual navigation. Nature Neuroscience. 2010 Nov; 13(11):1433–1440. https://doi.org/10.1038/nn.2648, doi: 10.1038/nn.2648.

Dong C, Madar AD, Sheffield MEJ. Distinct place cell dynamics in CA1 and CA3 encode experience in new environments. Nature Communications. 2021 May; 12(1):2977. https://doi.org/10.1038/s41467-021-23260-3, doi: 10.1038/s41467-021-23260-3.

Dragoi G, Tonegawa S. Preplay of future place cell sequences by hippocampal cellular assemblies. Nature. 2011 Jan; 469(7330):397–401. https://doi.org/10.1038/nature09633, doi: 10.1038/nature09633.

Driscoll LN, Duncker L, Harvey CD. Representational drift: Emerging theories for continual learning and experimental future directions. Current Opinion in Neurobiology. 2022; 76:102609. https://www.sciencedirect.com/science/article/pii/S0959438822001039, doi: https://doi.org/10.1016/j.conb.2022.102609.

Driscoll LN, Pettit NL, Minderer M, Chettih SN, Harvey CD. Dynamic Reorganization of Neuronal Activity Patterns in Parietal Cortex. Cell. 2017 Aug; 170(5):986–999.e16.

Ester M, Kriegel HP, Sander J, Xu X. A Density-Based Algorithm for Discovering Clusters in Large Spatial Databases with Noise. In: *Proceedings of the Second International Conference on Knowledge Discovery and Data Mining* KDD'96, AAAI Press; 1996. p. 226–231.

Foster DJ, Wilson MA. Reverse replay of behavioural sequences in hippocampal place cells during the awake state. Nature. 2006 Mar; 440(7084):680–683. https://doi.org/10.1038/nature04587, doi: 10.1038/nature04587.

Frank LM, Stanley GB, Brown EN. Hippocampal Plasticity across Multiple Days of Exposure to Novel Environments. Journal of Neuroscience. 2004; 24(35):7681–7689. https://www.jneurosci.org/content/24/35/7681, doi: 10.1523/JNEUROSCI.1958-04.2004.

Geva N, Deitch D, Rubin A, Ziv Y. Time and experience differentially affect distinct aspects of hippocampal representational drift. Neuron. 2023; https://www.sciencedirect.com/science/article/pii/S0896627323003781, doi: https://doi.org/10.1016/j.neuron.2023.05.005.

Gillespie AK, Astudillo Maya DA, Denovellis EL, Liu DF, Kastner DB, Coulter ME, Roumis DK, Eden UT, Frank LM. Hippocampal replay reflects specific past experiences rather than a plan for subsequent choice. Neuron. 2021 Oct; 109(19):3149–3163.e6. https://doi.org/10.1016/j.neuron.2021.07.029, doi: 10.1016/j.neuron.2021.07.029.

Gridchyn I, Schoenenberger P, O'Neill J, Csicsvari J. Assembly-Specific Disruption of Hippocampal Replay Leads to Selective Memory Deficit. Neuron. 2020; 106(2):291–300.e6. https://www.sciencedirect.com/science/article/pii/S0896627320300477, doi: https://doi.org/10.1016/j.neuron.2020.01.021.

Grienberger C, Milstein AD, Bittner KC, Romani S, Magee JC. Inhibitory suppression of heterogeneously tuned excitation enhances spatial coding in CA1 place cells. Nature Neuroscience. 2017 Mar; 20(3):417–426. https://doi.org/10.1038/nn.4486, doi: 10.1038/nn.4486.

Gupta AS, van der Meer MAA, Touretzky DS, Redish AD. Hippocampal Replay Is Not a Simple Function of Experience. Neuron. 2010; 65(5):695–705. https://www.sciencedirect.com/science/article/pii/S0896627310000607, doi: https://doi.org/10.1016/j.neuron.2010.01.034.

Guzman SJ, Schlögl A, Frotscher M, Jonas P. Synaptic mechanisms of pattern completion in the hippocampal CA3 network. Science. 2016; 353(6304):1117–1123. https://www.science.org/doi/abs/10.1126/science.aaf1836, doi: 10.1126/science.aaf1836.

Hainmueller T, Bartos M. Parallel emergence of stable and dynamic memory engrams in

the hippocampus. Nature. 2018 Jun; 558(7709):292–296. https://doi.org/10.1038/s41586-018-0191-2, doi: 10.1038/s41586-018-0191-2.

Ho J, Tumkaya T, Aryal S, Choi H, Claridge-Chang A. Moving beyond P values: data analysis with estimation graphics. Nature Methods. 2019 Jul; 16(7):565–566. https://doi.org/10.1038/s41592-019-0470-3, doi: 10.1038/s41592-019-0470-3.

Igata H, Ikegaya Y, Sasaki T. Prioritized experience replays on a hippocampal predictive map for learning. Proceedings of the National Academy of Sciences. 2021; 118(1):e2011266118. https://www.pnas.org/doi/abs/10.1073/pnas.2011266118, doi: 10.1073/pnas.2011266118.

Keinath AT, Mosser CA, Brandon MP. The representation of context in mouse hippocampus is preserved despite neural drift. Nature Communications. 2022 May; 13(1):2415. https://doi.org/10.1038/s41467-022-30198-7, doi: 10.1038/s41467-022-30198-7.

Khatib D, Ratzon A, Sellevoll M, Barak O, Morris G, Derdikman D. Active experience, not time, determines within-day representational drift in dorsal CA1. Neuron. 2023; https://www.sciencedirect.com/science/article/pii/S0896627323003872, doi: https://doi.org/10.1016/j.neuron.2023.05.014.

Knierim JJ, Neunuebel JP. Tracking the flow of hippocampal computation: Pattern separation, pattern completion, and attractor dynamics. Neurobiology of Learning and Memory. 2016; 129:38–49. https://www.sciencedirect.com/science/article/pii/S1074742715001884, doi: https://doi.org/10.1016/j.nlm.2015.10.008, pattern Separation and Pattern Completion in the Hippocampal System.

Krishnan S, Heer C, Cherian C, Sheffield MEJ. Reward expectation extinction restructures and degrades CA1 spatial maps through loss of a dopaminergic reward proximity signal.

Nature Communications. 2022 Nov; 13(1):6662. https://doi.org/10.1038/s41467-022-34465-5, doi: 10.1038/s41467-022-34465-5.

Lee I, Knierim JJ. The relationship between the field-shifting phenomenon and representational coherence of place cells in CA1 and CA3 in a cue-altered environment. Learning & Memory. 2007; 14(11):807–815. http://learnmem.cshlp.org/content/14/11/807.abstract, doi: 10.1101/lm.706207.

Lee JS, Briguglio JJ, Cohen JD, Romani S, Lee AK. The Statistical Structure of the Hippocampal Code for Space as a Function of Time, Context, and Value. Cell. 2020; 183(3):620–635.e22. https://www.sciencedirect.com/science/article/pii/S0092867420311650X, doi: https://doi.org/10.1016/j.cell.2020.09.024.

Leutgeb S, Leutgeb JK, Barnes CA, Moser EI, McNaughton BL, Moser MB. Independent Codes for Spatial and Episodic Memory in Hippocampal Neuronal Ensembles. Science. 2005; 309(5734):619–623. https://www.science.org/doi/abs/10.1126/science.1114037, doi: 10.1126/science.1114037.

Levy SJ, Hasselmo ME. Hippocampal remapping induced by new behavior is mediated by spatial context. eLife. 2023 jun; https://doi.org/10.7554/elife.87217.1, doi: 10.7554/elife.87217.1.

Mankin EA, Sparks FT, Slayyeh B, Sutherland RJ, Leutgeb S, Leutgeb JK. Neuronal code for extended time in the hippocampus. Proceedings of the National Academy of Sciences. 2012; 109(47):19462–19467. https://www.pnas.org/doi/abs/10.1073/pnas.1214107109, doi: 10.1073/pnas.1214107109.

Mankin E, Diehl G, Sparks F, Leutgeb S, Leutgeb J. Hippocampal CA2 Activity Patterns Change over Time to a Larger Extent than between Spatial Contexts. Neuron.

2015 Jan; 85(1):190–201. https://doi.org/10.1016/j.neuron.2014.12.001, doi: 10.1016/j.neuron.2014.12.001.

Marks TD, Goard MJ. Stimulus-dependent representational drift in primary visual cortex. Nature Communications. 2021 Aug; 12(1):5169. https://doi.org/10.1038/s41467-021-25436-3, doi: 10.1038/s41467-021-25436-3.

Mau W, Hasselmo ME, Cai DJ. The brain in motion: How ensemble fluidity drives memory-updating and flexibility. eLife. 2020 dec; 9:e63550. https://doi.org/10.7554/eLife.63550, doi: 10.7554/eLife.63550.

Mehta MR, Quirk MC, Wilson MA. Experience-dependent asymmetric shape of hippocampal receptive fields. Neuron. 2000 Mar; 25(3):707–715.

Miller KD. Synaptic Economics: Competition and Cooperation in Synaptic Plasticity. Neuron. 1996; 17(3):371–374. https://www.sciencedirect.com/science/article/pii/S0896627300801695, doi: https://doi.org/10.1016/S0896-6273(00)80169-5.

Moita MAP, Rosis S, Zhou Y, LeDoux JE, Blair HT. Putting Fear in Its Place: Remapping of Hippocampal Place Cells during Fear Conditioning. Journal of Neuroscience. 2004; 24(31):7015–7023. https://www.jneurosci.org/content/24/31/7015, doi: 10.1523/JNEUROSCI.5492-03.2004.

Morris RGM, Garrud P, Rawlins JNP, O'Keefe J. Place navigation impaired in rats with hippocampal lesions. Nature. 1982 Jun; 297(5868):681–683. https://doi.org/10.1038/297681a0, doi: 10.1038/297681a0.

Mou X, Pokhrel A, Suresh P, Ji D. Observational learning promotes hippocampal remote awake replay toward future reward locations. Neuron. 2022; 110(5):891–902.e7. https://www.sciencedirect.com/science/article/pii/S0896627321010138, doi: https://doi.org/10.1016/j.neuron.2021.12.005.

Nakazawa K, Quirk MC, Chitwood RA, Watanabe M, Yeckel MF, Sun LD, Kato A, Carr CA, Johnston D, Wilson MA, Tonegawa S. Requirement for Hippocampal CA3 NMDA Receptors in Associative Memory Recall. Science. 2002 Jul; 297(5579):211–218. https://doi.org/10.1126/science.1071795, doi: 10.1126/science.1071795.

O'Keefe J, Dostrovsky J. The hippocampus as a spatial map. Preliminary evidence from unit activity in the freely-moving rat. Brain Research. 1971; 34(1):171–175. https://www.sciencedirect.com/science/article/pii/0006899371903581, doi: https://doi.org/10.1016/0006-8993(71)90358-1.

Ólafsdóttir HF, Barry C, Saleem AB, Hassabis D, Spiers HJ. Hippocampal place cells construct reward related sequences through unexplored space. eLife. 2015 Jun; 4:e06063. https://doi.org/10.7554/eLife.06063, doi: 10.7554/eLife.06063, eLife 2015;4:e06063.

Pachitariu M, Stringer C, Dipoppa M, Schröder S, Rossi LF, Dalgleish H, Carandini M, Harris KD. Suite2p: beyond 10,000 neurons with standard two-photon microscopy. bioRxiv. 2017; https://www.biorxiv.org/content/early/2017/07/20/061507, doi: 10.1101/061507.

Pettit NL, Yuan XC, Harvey CD. Hippocampal place codes are gated by behavioral engagement. Nature Neuroscience. 2022 May; 25(5):561–566. https://doi.org/10.1038/s41593-022-01050-4, doi: 10.1038/s41593-022-01050-4.

Ratigan HC, Krishnan S, Smith S, Sheffield MEJ. Direct Thalamic Inputs to Hippocampal CA1 Transmit a Signal That Suppresses Ongoing Contextual Fear Memory Retrieval. bioRxiv. 2023; https://www.biorxiv.org/content/early/2023/03/27/2023.03.27.534420, doi: 10.1101/2023.03.27.534420.

Rebola N, Carta M, Mulle C. Operation and plasticity of hippocampal CA3 circuits:

implications for memory encoding. Nature Reviews Neuroscience. 2017 Apr; 18(4):208–220. https://doi.org/10.1038/nrn.2017.10, doi: 10.1038/nrn.2017.10.

Riedel G, Micheau J, Lam AGM, Roloff EvL, Martin SJ, Bridge H, Hoz Ld, Poeschel B, McCulloch J, Morris RGM. Reversible neural inactivation reveals hippocampal participation in several memory processes. Nature Neuroscience. 1999 Oct; 2(10):898–905. https://doi.org/10.1038/13202, doi: 10.1038/13202.

Roth ED, Yu X, Rao G, Knierim JJ. Functional Differences in the Backward Shifts of CA1 and CA3 Place Fields in Novel and Familiar Environments. PLOS ONE. 2012 04; 7(4):1–10. https://doi.org/10.1371/journal.pone.0036035, doi: 10.1371/journal.pone.0036035.

Roth ED, Yu X, Rao G, Knierim JJ. Functional Differences in the Backward Shifts of CA1 and CA3 Place Fields in Novel and Familiar Environments. PLOS ONE. 2012 04; 7(4):1–10. https://doi.org/10.1371/journal.pone.0036035, doi: 10.1371/journal.pone.0036035.

Rubin A, Geva N, Sheintuch L, Ziv Y. Hippocampal ensemble dynamics timestamp events in long-term memory. eLife. 2015 dec; 4:e12247. https://doi.org/10.7554/eLife.12247, doi: 10.7554/eLife.12247.

Sadowski JLP, Jones M, Mellor J. Sharp-Wave Ripples Orchestrate the Induction of Synaptic Plasticity during Reactivation of Place Cell Firing Patterns in the Hippocampus. Cell Reports. 2016 Mar; 14(8):1916–1929. https://doi.org/10.1016/j.celrep.2016.01.061, doi: 10.1016/j.celrep.2016.01.061.

Schoonover CE, Ohashi SN, Axel R, Fink AJP. Representational drift in primary olfactory cortex. Nature. 2021 Jun; 594(7864):541–546. https://doi.org/10.1038/s41586-021-03628-7, doi: 10.1038/s41586-021-03628-7.

Schröder H, Moser N, Huggenberger S. 11. In: The Mouse Hippocampus Cham: Springer International Publishing; 2020. p. 267–288. https://doi.org/10.1007/978-3-030-19898-5_11, doi: 10.1007/978-3-030-19898-5_11.

Schuette PJ, Reis FMCV, Maesta-Pereira S, Chakerian M, Torossian A, Blair GJ, Wang W, Blair HT, Fanselow MS, Kao JC, Adhikari A. Long-Term Characterization of Hippocampal Remapping during Contextual Fear Acquisition and Extinction. Journal of Neuroscience. 2020; 40(43):8329–8342. https://www.jneurosci.org/content/40/43/8329, doi: 10.1523/JNEUROSCI.1022-20.2020.

Scoville WB, Milner B. Loss of recent memory after bilateral hippocampal lesions. J Neurol Neurosurg Psychiatry. 1957 Feb; 20(1):11–21.

Sheffield MEJ, Dombeck DA. Calcium transient prevalence across the dendritic arbour predicts place field properties. Nature. 2015 Jan; 517(7533):200–204. https://doi.org/10.1038/nature13871, doi: 10.1038/nature13871.

Sheffield MEJ, Adoff MD, Dombeck DA. Increased Prevalence of Calcium Transients across the Dendritic Arbor during Place Field Formation. Neuron. 2017; 96(2):490–504.e5. https://www.sciencedirect.com/science/article/pii/S0896627317308735, doi: https://doi.org/10.1016/j.neuron.2017.09.029.

Sheffield ME, Dombeck DA. Dendritic mechanisms of hippocampal place field formation. Current Opinion in Neurobiology. 2019; 54:1–11. https://www.sciencedirect.com/science/article/pii/S0959438818300734, doi: https://doi.org/10.1016/j.conb.2018.07.004, neurobiology of Learning and Plasticity.

Shin JD, Tang W, Jadhav SP. Dynamics of Awake Hippocampal-Prefrontal Replay for Spatial Learning and Memory-Guided Decision Making. Neuron. 2019; 104(6):1110–1125.e7.

https://www.sciencedirect.com/science/article/pii/S0896627319307858, doi: https://doi.org/10.1016/j.neuron.2019.09.012.

Singer AC, Carr MF, Karlsson MP, Frank LM. Hippocampal SWR Activity Predicts Correct Decisions during the Initial Learning of an Alternation Task. Neuron. 2013 Mar; 77(6):1163–1173. https://doi.org/10.1016/j.neuron.2013.01.027, doi: 10.1016/j.neuron.2013.01.027.

Singer AC, Frank LM. Rewarded Outcomes Enhance Reactivation of Experience in the Hippocampus. Neuron. 2009 Dec; 64(6):910–921. https://doi.org/10.1016/j.neuron.2009.11.016, doi: 10.1016/j.neuron.2009.11.016.

Skaggs WE, McNaughton BL. Replay of Neuronal Firing Sequences in Rat Hippocampus During Sleep Following Spatial Experience. Science. 1996; 271(5257):1870–1873. https://www.science.org/doi/abs/10.1126/science.271.5257.1870, doi: 10.1126/science.271.5257.1870.

Vago DR, Wallenstein GV, Morris LS. Hippocampus. In: *Reference Module in Neuroscience and Biobehavioral Psychology* Elsevier; 2017.p. 566–570. https://www.sciencedirect.com/science/article/pii/B9780128093245045387, doi: https://doi.org/10.1016/B978-0-12-809324-5.04538-7.

Widloski J, Foster DJ. Flexible rerouting of hippocampal replay sequences around changing barriers in the absence of global place field remapping. Neuron. 2022; 110(9):1547–1558.e8. https://www.sciencedirect.com/science/article/pii/S089662732200109X, doi: https://doi.org/10.1016/j.neuron.2022.02.002.

Wilson MA, McNaughton BL. Dynamics of the Hippocampal Ensemble Code for Space. Science. 1993; 261(5124):1055–1058. https://www.science.org/doi/abs/10.1126/science.8351520, doi: 10.1126/science.8351520.

Wilson MA, McNaughton BL. Reactivation of Hippocampal Ensemble Memories During Sleep. Science. 1994; 265(5172):676–679. https://www.science.org/doi/abs/10.1126/science.8036517, doi: 10.1126/science.8036517.

Wu CT, Haggerty D, Kemere C, Ji D. Hippocampal awake replay in fear memory retrieval. Nature Neuroscience. 2017 Apr; 20(4):571–580. https://doi.org/10.1038/nn.4507, doi: 10.1038/nn.4507.

Zemla R, Basu J. Hippocampal function in rodents. Current Opinion in Neurobiology. 2017; 43:187–197. https://www.sciencedirect.com/science/article/pii/S0959438817301071, doi: https://doi.org/10.1016/j.conb.2017.04.005, neurobiology of Learning and Plasticity.

Zheng C, Hwaun E, Loza CA, Colgin LL. Hippocampal place cell sequences differ during correct and error trials in a spatial memory task. Nature Communications. 2021 Jun; 12(1):3373. https://doi.org/10.1038/s41467-021-23765-x, doi: 10.1038/s41467-021-23765-x.

Ziv Y, Burns LD, Cocker ED, Hamel EO, Ghosh KK, Kitch LJ, Gamal AE, Schnitzer MJ. Long-term dynamics of CA1 hippocampal place codes. Nature Neuroscience. 2013 Mar; 16(3):264–266. https://doi.org/10.1038/nn.3329, doi: 10.1038/nn.3329.

Zutshi I, Valero M, Fernández-Ruiz A, Buzsáki G. Extrinsic control and intrinsic computation in the hippocampal CA1 circuit. Neuron. 2022 Feb; 110(4):658–673.e5. https://doi.org/10.1016/j.neuron.2021.11.015, doi: 10.1016/j.neuron.2021.11.015.

Ólafsdóttir HF, Bush D, Barry C. The Role of Hippocampal Replay in Memory and Planning. Current Biology. 2018; 28(1):R37–R50. https://www.sciencedirect.com/science/article/pii/S0960982217314410, doi: https://doi.org/10.1016/j.cub.2017.10.073.